THE ASTROPHYSICAL JOURNAL, 397:277–303, 1992 September 20

PHOTOMETRY, POLARIMETRY, SPECTROSCOPY, AND SPECTROPOLARIMETRY OF THE ENIGMATIC WOLF-RAYET STAR EZ CANIS MAJORIS

CARMELLE ROBERT[1,2]
Space Telescope Science Institute, 3700 San Martin Drive, Baltimore, MD 21218

ANTHONY F. J. MOFFAT[3,4,5]
Département de Physique, Université de Montréal, and Observatoire du mont Mégantic, C.P. 6128, Succ. A, Montréal, Québec, Canada H3C 3J7

LAURENT DRISSEN[2]
Space Telescope Science Institute, 3700 San Martin Drive, Baltimore, MD 21218

ROBERT LAMONTAGNE
Département de Physique, Université de Montréal, and Observatoire du mont Mégantic, C.P. 6128, Succ. A, Montréal, Québec, Canada H3C 3J7

WILHELM SEGGEWISS[4,6]
Observatorium Hoher List, Universitäts-Sternwarte Bonn, 5568 Daun, Germany

VIRPI S. NIEMELA[7] AND MIGUEL A. CERRUTI[8]
Instituto de Astronomia y Física del Espacio, Casilla de Correo 67, Succ. 28, 1428 Buenos Aires, Argentina

PAUL BARRETT[9]
NASA/Goddard Space Flight Center, Greenbelt, MD 20771

JEREMY BAILEY[1]
United Kingdom Infrared Telescope, Hawaii Headquarters, 665 Komohana Street, Hilo, HI 96720

JORGE GARCIA[2]
University of Toronto Southern Observatory, Las Campanas, Chile

AND

SANTIAGO TAPIA[2]
Lincoln Laboratory, MIT, Box 73, Lexington, MA 02173
Received 1991 March 18; accepted 1992 March 26

ABSTRACT

We present new multimode data collected since 1987 for the peculiar Wolf-Rayet star EZ CMa. The continuum photometry and polarimetry show periodic variations consistent with the previously known 3.766 day period. As before, the shapes of the light and polarization curves change from one epoch to another. A periodicity search was carried out on the amplitude of the light curves in an attempt to understand the epoch-to-epoch changes. The result was inconclusive.

Linear polarization data were well fitted with an eccentric binary model where an additional free parameter was included to allow for epoch-dependent changes of the geometrical electron distribution in the W-R envelope. This yielded a set of basic parameters including the eccentricity, $e = 0.39 \pm 0.02$, and the orbital inclination, $i = 114° \pm 3°$, which appear to remain constant within their errors for most data sets.

The spectroscopic data show global profile variations for all three observed strong emission lines He II λ5412, C IV λ5807, and He I λ5876. Periodicity of these variations was not obvious. Radial velocities of the lines vary with the 3.766 day period. Nevertheless, it is not clear whether these are strictly due to systematic line motion as expected in a binary system. Radially expanding inhomogeneities are also seen superposed on the line profiles. Variable polarization in the lines is also observed.

We searched for a correlation in the variability seen in different modes of observation; the situation is confused by a lack of sufficient simultaneity. Finally, we discuss all the results from two points of view: a W-R+c binary system and a rotating single star.

Subject headings: binaries: spectroscopic — polarization — stars: individual (EZ Canis Majoris) — stars: Wolf-Rayet

[1] Visiting Astronomer, AAT, Australia.
[2] Visiting Astronomer, University of Toronto Telescope, Las Campanas, Chile.
[3] Visiting Astronomer, MPI, La Silla, Chile.
[4] Visiting Astronomer, ESO, La Silla, Chile.
[5] Visiting Astronomer, CASLEO, Argentina.
[6] Visiting Astronomer, Bochum University Telescope, La Silla, Chile.
[7] Member of Carrera del Investigador, CIC, Prov. Buenos Aires, Argentina.
[8] Member of Carrera del Investigador, CONICET, Argentina.
[9] Astronomer, SAAO, South Africa.

1. INTRODUCTION

Variability of Wolf-Rayet (W-R) stars is a phenomenon which can be relatively well explained from a phenomenological point of view. Periodic variations are the signature of a binary system (all known such cases are W-R + O), while stochastic variations of W-R stars are associated with wind inhomogeneities (Moffat & Robert 1991). Nevertheless, the W-R star EZ CMa (HD 50896) avoids this simple rule. This bright WN5 (possibly WN4; Smith 1988) star shows periodic variations in almost all collected photometric, polarimetric, and spectroscopic data, with a period close to 3.766 days. However, EZ CMa is a special case in that these variations show strong epoch dependency and additional noise only in some modes of observation.

One of the first models to explain the peculiar behavior of EZ CMa was proposed by Firmani et al. (1980). They suggested that the periodic line profile, radial velocity, and continuum light variations are due to eccentric orbital motion in a binary system consisting of a W-R star and a neutron star (NS) companion. More recent refinements of the binary model, allowing for epoch changes, have been directed toward variable clouds in semi-corotation (van der Hucht, van Genderen, & Bakker 1990), density enhancements in the wind (Balona, Egan, & Marang 1989), or precession of an accreting disk around the compact companion (Drissen et al. 1989).

A major argument against the binary scenario for EZ CMa is the lack of strong X-ray emission (e.g., Pollock 1989), as expected when there is accretion onto a compact companion (unless the W-R wind effectively absorbs the X-rays; but see Stevens & Willis 1988). Also, the P Cygni profiles in the UV, studied by Willis et al. (1989), do not show any phase variations which could be due to the Hatchett-McCray effect (i.e., periodic modulation of the ionization structure in the wind due to an orbiting compact companion). New UV spectra display a 1 day periodicity, which has been claimed to be related to wind instabilities (St.-Louis 1990; St.-Louis et al. 1991). Consequently, a single rotating star is another possibility to consider. A single star with a rotating disk and magnetic filaments was proposed by Underhill & Yang (1991), based mainly on spectral features. Similarities between the spectropolarimetric data for EZ CMa collected by Schulte-Ladbeck et al. (1990) and those for Be stars support the idea of a rotating, expanding wind surrounding a single star.

EZ CMa shows other peculiarities (which are not restricted to this W-R star alone). It is located at a relatively large distance from the Galactic plane ($z = -274$ pc: van der Hucht et al. 1988), in the direction of the open cluster Collinder 121, and surrounded by a wind-blown bubble seen as a ring nebula, S308 (Chu et al. 1982). Even more interesting, a supernovae remnant (SNR) has been found to lie nearly concentric with EZ CMa (Nichols-Bohlin & Fesen 1986); if their distances are the same—a good possibility within the uncertainties—the SNR could be related to EZ CMa (Nichols-Bohlin & Fesen 1990).

In this paper we present new observations for EZ CMa collected since 1987. Data for different modes—photometry, polarimetry, spectroscopy, and spectropolarimetry—are discussed. The goal is to find new clues which will help solve the mystery relating to the true nature of EZ CMa.

2. OBSERVATIONS AND REDUCTION

Extensive multimode monitoring of EZ CMa was pursued again during the past 3 years. The observations in order of time are the following:

1. *1988 October 3–21.*—Photometric observations were obtained at the Bochum University 0.6 m telescope on La Silla, Chile. A single-channel photometer was used with the three filters Strömgren *b* and Johnson *B* and *V*. Linear polarimetric observations in Strömgren *b* and *y* filters were collected quasi-simultaneously using the polarimeter PISCO at the Max-Planck-Institut (MPI) 2.2 m telescope on La Silla.

2. *1988 November 25–28.*—Spectropolarimetric data were collected at the 3.9 m Anglo-Australian Telescope (AAT). A Pockels cell and two quarter-wave plates are the major components of the polarimetry module used. This apparatus was coupled to the RGO spectrograph and a CCD detector. The resolution is 1.43 Å pixel^{-1}. Spectral coverage extended from 5230 to 6050 Å.

3. *1989 February 16–18.*—Extensive time-sequence spectroscopy was the objective of this run. The observations were taken at the 1.6 m telescope of the Observatoire du mont Mégantic (OMM), Canada, with the spectrograph followed by a CCD detector. The spectral range covered extended from 5330 to 5980 Å with a resolution of 1.325 Å pixel^{-1}.

4. *1989 May 26–June 2.*—Photometric and spectroscopic measurements were carried out during this period. The photometer was attached to the European Southern Observatory (ESO) 0.5 m telescope on La Silla and equipped with Strömgren *b* and *y* filters. Three high-quality CCD spectra were collected on three successive nights at the ESO 3.6 m telescope (La Silla) with CASPEC. The echelle spectrograph covered the spectral range 5160–6190 Å with 0.07 Å pixel^{-1} resolution.

5. *1990 January 13–February 1 and March 19–27.*—Simultaneous photometry and linear polarimetry were undertaken during the first of these two periods, while only polarimetry was carried out in March. The VATPOL photopolarimeter was used at the CASLEO 2.15 m telescope in Argentina for both runs. A narrow-band filter centered at λ_c = 4770 Å (full width at half-maximum [FWHM] = 30 Å) was preferred over other standard filters to isolate the continuum light (i.e., to avoid the W-R emission lines).

6. *1990 February 5–March 1 and March 17–22.*—G-band (λ_c = 5388 Å and FWHM = 352 Å) photometric data and linear polarimetric data were collected simultaneously with the MINIPOL polarimeter at the 0.6 m telescope of the University of Toronto Southern Observatory (UTSO) on Las Campanas, Chile. More spectra were obtained at OMM in February with the same setup as in observation 3.

7. *1990 February 19–26 and March 20–April 1.*—The University of Cape Town photopolarimeter and a Johnson *V* filter were employed to obtain photometric data simultaneously with linear and circular polarimetric data. These observations were carried out at the South African Astronomical Observatory (SAAO) 1.0 m telescope.

The photometric data are listed in Tables 1A–1E. The same comparison star, C1 (HD 50853, spectral type A1), and the same control star, C2 (HD 50711, spectral type A2), were observed alternately with EZ CMa for all the photometric runs. Both stars are well known for their constancy (e.g., Drissen et al. 1989). The mean error for each photometric point is ~0.004 mag (somewhat worse, ~0.007 mag, in the narrower continuum filter centered at 4770 Å), estimated from the standard deviation from the mean of the magnitudes C2 − C1.

Tables 2A–2E give the polarimetric observations with *P*, the degree of linear polarization; Θ, the angle of polarization in the equatorial system; and *V*, the degree of circular polarization. Respective errors are given by ρ_P, σ_Θ, and σ_V. Table 2B con-

TABLE 1A

PHOTOMETRY 1988 (Bochum 0.6 m)

JD −2,447.000.0	φ	W-R − C1 b (mag)	W-R − C1 B (mag)	W-R − C1 V (mag)	C2 − C1 b (mag)	C2 − C1 B (mag)	C2 − C1 V (mag)
437.881	0.017	−0.389	0.384	0.672	0.320	0.373	0.313
438.856	0.276	−0.413	0.334	0.619	0.331	0.369	0.314
439.815	0.531	−0.396	0.378	0.675	0.321	0.373	0.308
440.847	0.805	−0.383	0.396	0.684	0.328	0.374	0.311
441.876	0.078	−0.395	0.375	0.658	0.322	0.376	0.310
442.840	0.334	−0.424	0.317	0.596	0.330	0.374	0.308
443.860	0.605	−0.382	0.388	0.686	0.325	0.369	0.311
444.863	0.871	−0.407	0.385	0.675	...	...	...
445.872	0.139	−0.398	0.364	0.662	0.325	0.375	0.322
446.885	0.408	−0.426	0.348	0.635	0.323	0.370	0.308
447.874	0.671	−0.389	0.388	0.674	0.321	0.375	0.317
448.869	0.935	−0.396	0.384	0.672	0.321	0.368	0.306
449.863	0.199	−0.400	0.365	0.656	0.328	0.374	0.312
450.847	0.460	−0.405	0.366	0.654	0.324	0.364	0.313
451.842	0.724	−0.396	0.377	0.669	0.326	0.370	0.309
452.878	0.999	−0.394	0.374	0.660	0.326	0.372	0.306
453.862	0.261	−0.416	0.333	0.619	0.323	0.368	0.307
454.836	0.519	−0.399	0.371	0.660	0.325	0.368	0.306
455.776	0.769	−0.397	0.369	0.662	0.322	0.360	0.302
Mean	...	−0.400	0.368	0.657	0.325	0.371	0.310
σ	...	0.012	0.021	0.024	0.003	0.004	0.005

NOTE.—Phases, φ, are calculated with the ephemeris of LML: JD 2,446, 153.61 + 3.766E.

tains the polarimetric parameters extracted from the continuum part of the AAT spectropolarimetric data. The nightly averaged polarization spectrum was used in order to improve the Poisson error of each data point. For all the polarimetric runs, the instrumental polarization was measured by observing unpolarized standard stars; this yielded negligible corrections in all but a few cases, in which appropriate subtraction was applied. The uncertainty in the origin of the position angle was estimated to be less than 1°, using polarized standard stars and the internal calibration of the polarimeters when possible. Circular polarization was calibrated via observation of magnetic stars of known level.

Exposure times for spectroscopy, $\sim$10 minutes per spectrum on average for all spectroscopic runs at AAT, ESO, and OMM, were chosen to give a signal-to-noise ratio (S/N) of 200–250 pixel^{-1} in the continuum and up to 400 in the strongest emission lines. Continuum lamp exposures were made each night in order to remove pixel-to-pixel sensitivity variations. The comparison arc for wavelength calibration was Th at ESO and

TABLE 1B

PHOTOMETRY 1989 (ESO 0.5 m)

JD −2,447,000.0	φ	W-R − C1 b (mag)	W-R − C1 y (mag)	C2 − C1 b (mag)	C2 − C1 y (mag)
673.468	0.574	−0.388	0.441	0.326	0.290
674.475	0.841	−0.380	0.451	0.325	0.292
676.471	0.371	−0.387	0.437	0.326	0.298
677.465	0.635	−0.396	0.436	0.327	0.300
678.475	0.903	−0.392	0.422	0.321	0.289
680.474	0.434	−0.387	0.446	0.330	0.293
Mean	...	−0.388	0.439	0.326	0.294
σ	...	0.005	0.010	0.003	0.004

NOTE.—Phases, φ, are as in Table 1A.

TABLE 1C

PHOTOMETRY 1990 (CASLEO 2.15 m)

JD −2,447,000.0	φ	λ4770 W-R − C1 (mag)	λ4770 C2 − C1 (mag)
904.589	0.944	0.806	...
905.790	0.263	0.796	0.320
905.815	0.270	0.788	...
906.687	0.501	0.768	...
907.653	0.758	0.810	0.309
907.836	0.806	0.823	...
908.649	0.022	0.783	0.312
908.651	0.023	0.786	...
909.664	0.292	0.786	0.310
910.559	0.592	0.780	...
910.809	0.596	0.796	...
911.810	0.861	0.814	0.324
912.805	0.126	0.789	0.325
916.809	0.189	0.821	0.320
917.692	0.423	0.767	0.326
917.823	0.458	0.782	...
920.775	0.242	0.794	0.317
921.712	0.491	0.784	0.330
921.719	0.493	0.784	0.318
Mean	...	0.793	0.319
σ	...	0.016	0.007

NOTE.—Phase, φ, are as in Table 1A.

TABLE 1D

PHOTOMETRY 1990 (UTSO 0.6 m)

JD −2,447,000.0	φ	G FILTER W-R − C1 (mag)	G FILTER C2 − C1 (mag)
930.554	0.839	0.555	0.299
930.703	0.878	0.573	0.301
931.559	0.105	0.539	0.298
931.717	0.147	0.567	0.298
932.548	0.368	0.541	0.292
932.693	0.407	0.544	0.305
934.562	0.903	0.579	0.301
934.690	0.937	0.578	0.294
935.554	0.166	0.581	0.290
935.692	0.203	0.571	0.299
937.555	0.698	0.532	0.298
937.692	0.734	0.536	0.300
938.594	0.973	0.564	0.295
938.697	0.001	0.558	0.302
939.555	0.229	0.559	0.297
940.570	0.498	0.547	0.293
940.688	0.529	0.580	0.301
943.546	0.288	0.547	0.303
943.687	0.326	0.533	0.301
944.551	0.555	0.558	0.296
944.687	0.591	0.546	0.301
945.548	0.820	0.563	0.305
946.551	0.086	0.538	0.305
947.541	0.349	0.515	0.301
947.653	0.379	0.520	...
948.545	0.616	0.542	0.303
949.553	0.883	0.562	0.302
951.551	0.414	0.522	0.301
967.514	0.653	0.533	...
969.514	0.184	0.561	...
970.513	0.449	0.543	...
971.514	0.715	0.515	...
Mean	...	0.550	0.299
σ	...	0.019	0.004

NOTE.—Phases, φ, are as in Table 1A.

TABLE 1E

PHOTOMETRY 1990 (SAAO 1.0 m)

JD −2,447,000.0	φ	V FILTER W-R − C1 (mag)	V FILTER C2 − C1 (mag)
944.382	0.510	0.612	0.308
944.470	0.534	0.601	0.316
945.322	0.760	0.633	0.310
946.317	0.024	0.613	0.314
946.417	0.051	0.600	0.309
946.470	0.065	0.609	0.318
948.325	0.557	0.628	0.306
948.436	0.587	0.629	0.308
949.306	0.818	0.639	0.301
949.396	0.842	0.635	0.308
949.459	0.858	0.657	0.317
972.272	0.916	0.614	0.302
973.281	0.184	0.630	0.302
976.288	0.982	0.612	0.310
977.257	0.240	0.609	0.306
977.385	0.274	0.596	0.310
978.291	0.514	0.633	0.316
979.280	0.777	0.606	0.305
979.388	0.806	0.632	0.311
981.257	0.302	0.587	0.305
982.364	0.596	0.629	0.310
983.261	0.834	0.638	0.307
Mean	...	0.620	0.309
σ	...	0.017	0.005

NOTE.—Phases, φ, are as in Table 1A.

TABLE 2A

LINEAR POLARIMETRY 1988 (MPI 2.2 m)

JD −2,447,000.0	φ	P (%)	σ_P (%)	Θ	σ_Θ
b Filter					
439.876	0.547	0.370	0.015	163°2	1°1
440.874	0.812	0.435	0.019	155.9	1.3
441.880	0.070	0.310	0.013	154.0	1.2
442.878	0.344	0.380	0.013	156.5	1.0
443.889	0.613	0.340	0.017	164.6	1.4
444.893	0.879	0.447	0.017	153.3	1.1
445.888	0.143	0.364	0.016	155.5	1.3
446.867	0.403	0.393	0.013	156.9	0.9
447.885	0.674	0.447	0.016	158.8	1.0
448.891	0.941	0.379	0.030	153.5	2.3
449.872	0.201	0.350	0.014	164.9	1.1
450.881	0.469	0.395	0.022	160.4	1.6
451.883	0.735	0.416	0.017	159.6	1.2
452.880	0.000	0.359	0.015	151.9	1.2
y Filter					
439.886	0.550	0.426	0.021	163°3	1°4
440.884	0.815	0.565	0.023	151.3	1.2
441.891	0.082	0.246	0.016	151.2	1.9
442.888	0.347	0.344	0.016	150.5	1.3
443.880	0.610	0.491	0.021	164.1	1.2
444.882	0.876	0.552	0.020	149.0	1.0
445.879	0.141	0.328	0.018	157.3	1.6
446.876	0.406	0.460	0.016	154.8	1.0
447.876	0.671	0.610	0.022	158.6	1.0
448.884	0.939	0.499	0.027	143.9	1.6
449.886	0.205	0.326	0.021	165.3	1.8
450.872	0.467	0.490	0.024	161.2	1.4
451.874	0.733	0.570	0.023	157.5	1.2
452.872	0.998	0.346	0.020	144.0	1.7

NOTE.—Phases, φ, are as in Table 1A.

TABLE 2B

LINEAR POLARIMETRY 1988 (AAT 3.9 m): CONTINUUM, 5500–5730 Å

JD −2,447,000.0	φ	P (%)	σ_P (%)	Θ	σ_Θ
491.219	0.181	0.478	0.053	129°8	3°2
492.169	0.433	0.598	0.045	146.6	2.2
493.167	0.698	0.696	0.024	156.7	1.0
494.181	0.967	0.675	0.034	142.3	1.4

NOTE.—Phases, φ, are as in Table 1A.

Cu-Ar at the other observatories. No flux calibration was carried out; rather, the spectra were rectified using the continuum as a reference. All spectra were rectified with a low-order (usually fourth-order) Legendre polynomial and a set of seven fixed windows in the continuum. The spectropolarimetric data were reduced using the special ADAM package TSP and FIGARO at AAT. Extraction of the echelle spectra from ESO was done at Munich with MIDAS. The IRAF routines at the Université de Montréal were used for the OMM spectroscopy and final reduction of the AAT and ESO spectra. Table 3 presents the journal of observations for the spectroscopic runs.

Probably because of the polarimeter optics, ripples appeared in the final intensity spectra from the AAT. The peak-to-valley amplitude of the ripples was ~3% of the continuum level. The

TABLE 2C

LINEAR POLARIMETRY 1990 (CASLEO 2.15 m): NARROW-BAND λ4770 FILTER (continuum)

JD −2,447,000.0	φ	P (%)	σ_P (%)	Θ	σ_Θ
904.589	0.944	1.019	0.040	134°0	1°1
905.790	0.263	0.560	0.035	142.0	1.8
905.815	0.270	0.570	0.037	141.7	1.9
906.687	0.501	0.712	0.032	150.0	1.3
907.622	0.749	1.038	0.058	156.8	1.6
907.640	0.754	0.998	0.032	153.1	0.9
907.852	0.810	1.123	0.032	146.7	0.8
908.658	0.024	0.753	0.033	131.1	1.3
908.864	0.079	0.569	0.075	133.5	3.8
909.672	0.294	0.489	0.035	143.6	2.1
910.559	0.529	0.791	0.041	152.7	1.5
910.819	0.598	0.815	0.038	149.5	1.3
911.820	0.864	1.162	0.032	141.0	0.8
912.815	0.128	0.748	0.033	133.9	1.3
913.659	0.352	0.582	0.050	143.0	2.5
913.817	0.394	0.595	0.041	137.9	2.0
913.848	0.403	0.719	0.073	142.7	2.9
914.647	0.615	0.709	0.041	154.9	1.7
915.797	0.920	0.987	0.042	135.6	1.2
916.799	0.186	0.678	0.038	135.1	1.6
917.658	0.414	0.589	0.032	143.9	1.6
917.833	0.461	0.828	0.036	152.0	1.2
919.788	0.980	0.898	0.037	130.2	1.2
920.784	0.244	0.635	0.040	137.8	1.8
921.728	0.495	0.630	0.030	143.5	1.4
923.806	0.047	0.587	0.050	131.9	2.4
969.545	0.192	0.542	0.029	135.4	1.5
970.531	0.454	0.459	0.035	146.1	2.2
971.567	0.729	1.157	0.035	152.4	0.9
971.606	0.739	1.160	0.045	152.1	1.1
973.527	0.249	0.516	0.030	138.5	1.7
974.560	0.524	0.674	0.036	152.8	1.5
975.547	0.786	1.202	0.036	149.6	0.9
976.606	0.067	0.624	0.030	134.0	1.4
977.574	0.324	0.397	0.028	124.5	2.0

NOTE.—Phases, φ, are as in Table 1A.

TABLE 2D

LINEAR POLARIMETRY 1990 (UTSO 0.6 m): G FILTER

JD −2,447,000.0	φ	P (%)	σ_P (%)	Θ	σ_Θ	JD −2,447,000.0	φ	P (%)	σ_P (%)	Θ	σ_Θ
927.618	0.059	0.552	0.026	135°9	1°3	941.538	0.755	0.934	0.022	154.6	0.7
928.553	0.307	0.518	0.023	142.8	1.3	941.679	0.793	1.028	0.024	151.7	0.7
928.688	0.343	0.483	0.024	145.4	1.4	942.549	0.024	0.674	0.020	132.0	0.9
929.582	0.580	0.695	0.020	153.9	0.8	942.696	0.063	0.617	0.035	137.9	1.6
930.534	0.833	1.028	0.032	143.8	0.9	943.592	0.284	0.556	0.018	140.2	0.9
930.723	0.883	1.050	0.038	140.8	1.0	943.715	0.333	0.480	0.021	140.8	1.3
931.536	0.099	0.603	0.024	138.6	1.1	944.527	0.549	0.649	0.021	156.8	0.9
931.695	0.142	0.693	0.023	138.8	1.0	944.712	0.598	0.714	0.025	154.0	1.0
932.528	0.363	0.551	0.020	141.8	1.0	945.530	0.815	1.025	0.023	147.8	0.6
932.714	0.412	0.621	0.022	138.3	1.0	946.528	0.080	0.478	0.024	138.5	1.4
933.588	0.636	0.800	0.021	152.7	0.8	946.689	0.123	0.570	0.029	139.3	1.5
934.541	0.897	1.067	0.023	139.6	0.6	947.525	0.345	0.501	0.015	137.9	0.9
934.707	0.941	0.981	0.024	136.1	0.7	948.568	0.622	0.709	0.011	157.8	0.4
935.534	0.161	0.585	0.017	140.5	0.8	949.530	0.877	1.036	0.020	144.7	0.6
935.709	0.207	0.617	0.020	138.9	0.9	950.527	0.142	0.603	0.021	140.0	1.0
936.553	0.431	0.539	0.036	144.9	1.9	951.532	0.409	0.626	0.016	143.2	0.7
937.537	0.693	0.853	0.022	153.9	0.7	967.514	0.653	0.907	0.016	156.9	0.5
937.711	0.739	0.838	0.018	152.5	0.6	968.522	0.920	0.999	0.019	143.8	0.5
938.566	0.966	0.904	0.002	135.8	0.7	968.622	0.947	0.292	0.036	139.2	1.1
938.714	0.005	0.802	0.029	135.2	1.0	969.514	0.184	0.516	0.021	140.1	1.2
939.536	0.224	0.554	0.013	138.2	0.7	970.513	0.449	0.476	0.017	150.7	1.0
939.677	0.261	0.571	0.045	138.8	2.3	971.514	0.715	0.998	0.019	153.4	0.5
940.549	0.493	0.519	0.017	149.2	0.9	972.524	0.983	0.745	0.021	137.1	0.8
940.715	0.537	0.574	0.024	153.7	1.2						

NOTE.—Phases, φ, are as in Table 1A.

TABLE 2E

LINEAR AND CIRCULAR POLARIMETRY 1990 (SAAO 1.0 m): V FILTER

JD −2,447,000.0	φ	P (%)	σ_P (%)	Θ	σ_Θ	V (%)	σ_V (%)
942.348	0.970	0.875	0.020	134°0	0°7	0.019	0.014
942.423	0.990	0.857	0.021	130.3	0.7	0.007	0.015
944.302	0.489	0.593	0.019	149.6	0.9	0.019	0.013
944.396	0.514	0.648	0.022	154.9	1.0	0.000	0.015
944.483	0.537	0.647	0.023	155.7	1.0	0.029	0.016
945.336	0.764	1.053	0.020	149.0	0.5	0.001	0.014
945.404	0.782	1.044	0.023	150.4	0.6	0.043	0.017
945.464	0.798	1.090	0.020	149.4	0.5	0.026	0.014
946.329	0.027	0.580	0.020	134.6	1.0	0.007	0.014
946.428	0.054	0.531	0.023	136.7	1.2	0.031	0.016
946.481	0.068	0.544	0.024	138.8	1.3	0.000	0.017
947.437	0.322	0.501	0.018	140.8	1.0	−0.022	0.013
948.339	0.561	0.687	0.018	155.6	0.8	−0.011	0.013
948.448	0.590	0.774	0.021	160.1	0.8	−0.033	0.015
949.320	0.822	1.166	0.020	147.0	0.5	0.020	0.014
949.409	0.845	1.130	0.021	145.9	0.5	−0.018	0.015
949.473	0.862	1.091	0.021	146.0	0.6	0.023	0.015
971.389	0.682	1.020	0.024	151.7	0.7	0.038	0.017
972.285	0.920	0.904	0.020	142.0	0.7	0.036	0.014
972.400	0.950	0.900	0.019	140.4	0.6	0.005	0.013
973.293	0.187	0.571	0.021	144.5	1.1	0.005	0.015
976.301	0.986	0.836	0.020	138.9	0.7	0.019	0.014
976.409	0.015	0.658	0.027	139.4	1.2	0.024	0.019
977.269	0.243	0.536	0.020	133.6	1.1	0.034	0.014
977.398	0.277	0.461	0.019	134.7	1.2	0.014	0.015
978.304	0.518	0.731	0.018	156.8	0.7	0.013	0.013
979.295	0.781	1.301	0.018	150.5	0.4	0.025	0.013
979.400	0.809	1.292	0.021	149.2	0.5	0.057	0.015
980.307	0.050	0.630	0.019	137.4	0.9	0.006	0.014
981.269	0.305	0.523	0.020	136.4	1.1	0.002	0.014
982.377	0.599	0.922	0.019	159.8	0.6	0.006	0.014
983.274	0.837	1.135	0.019	147.8	0.5	0.041	0.013
Mean	...	...	...	...	...	0.014 ± 0.003	0.015
σ	...	...	...	...	...	0.020	...

NOTE.—Phases, φ, are as in Table 1A.

1992ApJ...397..277R

TABLE 3

JOURNAL OF THE SPECTROSCOPIC OBSERVATIONS

Observatory	Date	JD −2,447,000.0	Observatory	Date	JD −2,447,000.0	Observatory	Date	JD −2,447,000.0
AAT (3.9 m).....	1988 Nov 25	491.201	OMM (1.6 m).....	1989 Feb 17	575.645	OMM (1.6 m).....	1989 Feb 18	576.660
		491.236		1989 Feb 18	576.508			576.666
	1988 Nov 26	492.148			576.518			576.671
		492.190			576.524			576.678
	1988 Nov 27	493.099			576.536	ESO (3.6 m).....	1989 May 30	677.482
		493.155			576.541		1989 May 31	678.460
		493.195			576.545		1989 Jun 1	679.455
		493.235			576.550	OMM (1.6 m).....	1990 Feb 9	931.584
	1988 Nov 28	494.127			576.554			931.594
		494.174			576.559			931.626
		494.235			576.572			931.637
OMM (1.6 m).....	1989 Feb 16	574.562			576.577			931.728
		574.571			576.582		1990 Feb 13	935.605
		574.580			576.585			935.615
		574.585			576.591			935.628
		574.600			576.593			935.637
		574.606			576.596			935.663
		574.613			576.599			935.672
		574.620			576.602			935.685
		574.626			576.604			935.697
		574.632			576.618		1990 Feb 15	937.573
		574.640			576.620			937.581
		574.646			576.623			937.591
		574.653			576.626			937.601
	1989 Feb 17	575.603			576.629			937.619
		575.619			576.632			
		575.632			576.655			

ripple structure showed a variable period of ~50 Å. Ripples were not observed in the $Q(\lambda)$, $U(\lambda)$ spectra because the reduction method of the Stokes parameters employed a division of two spectra containing a similar ripple pattern. To eliminate the ripples on the intensity spectra, we first Fourier-analyzed the spectra themselves, then reduced the ripple power peaks to neighboring normal values, and finally Fourier-transformed back to the original coordinates. However, this procedure was not effective in separating the coefficients associated with the ripples from those related to the emission lines. Best results were thus obtained by applying the Fourier method to the spectra *after* their division by the OMM average spectrum to extract the ripple function (in this way the contribution from the emission lines is considerably reduced). The final spectrum was then obtained by dividing the original spectrum by the ripple function. This operation required the rebinning of the AAT spectra with the same resolution as for the OMM data.

After merging the different spectral orders obtained with the ESO echelle spectrograph, we found some residual ripples in the spectra. These were due not to interorder overlap problems but rather to discretization effects of the extraction process of spectra slightly inclined to the CCD axis. They were removed by dividing each spectrum by a low-order fit to the continuum of the flux standard Feige 110 observed with the same detector setup. (After completing this, we became aware of a more general method of dealing with this problem: Verschueren & Hensberge 1990.)

The air mass, X, for the spectra collected at OMM ranged between 2.6 and 4.9. Early A-type stars (HD 50853, [i.e., C1], type A2, and HD 46933, type A0 V) were observed at OMM when possible at the same air mass as for EZ CMa. This revealed telluric absorption features located between ~5860 Å and the end of the spectra; they are caused mainly by atmospheric H_2O. The maximum depth observed is 3.5% of the continuum for $X = 3$. The A star spectra were then used to correct this effect. The telescope was close to the zenith when observing at the AAT (maximum $X \simeq 1.2$), while $X \simeq 1.8$ at ESO.

3. RESULTS

3.1. *Individual Light Curves*

Figure 1 presents a montage of all the useful light curves of EZ CMa collected from the literature and including the present new data. (The high-quality observations of Balona et al. 1989, all carried out with a Strömgren *b* were omitted in

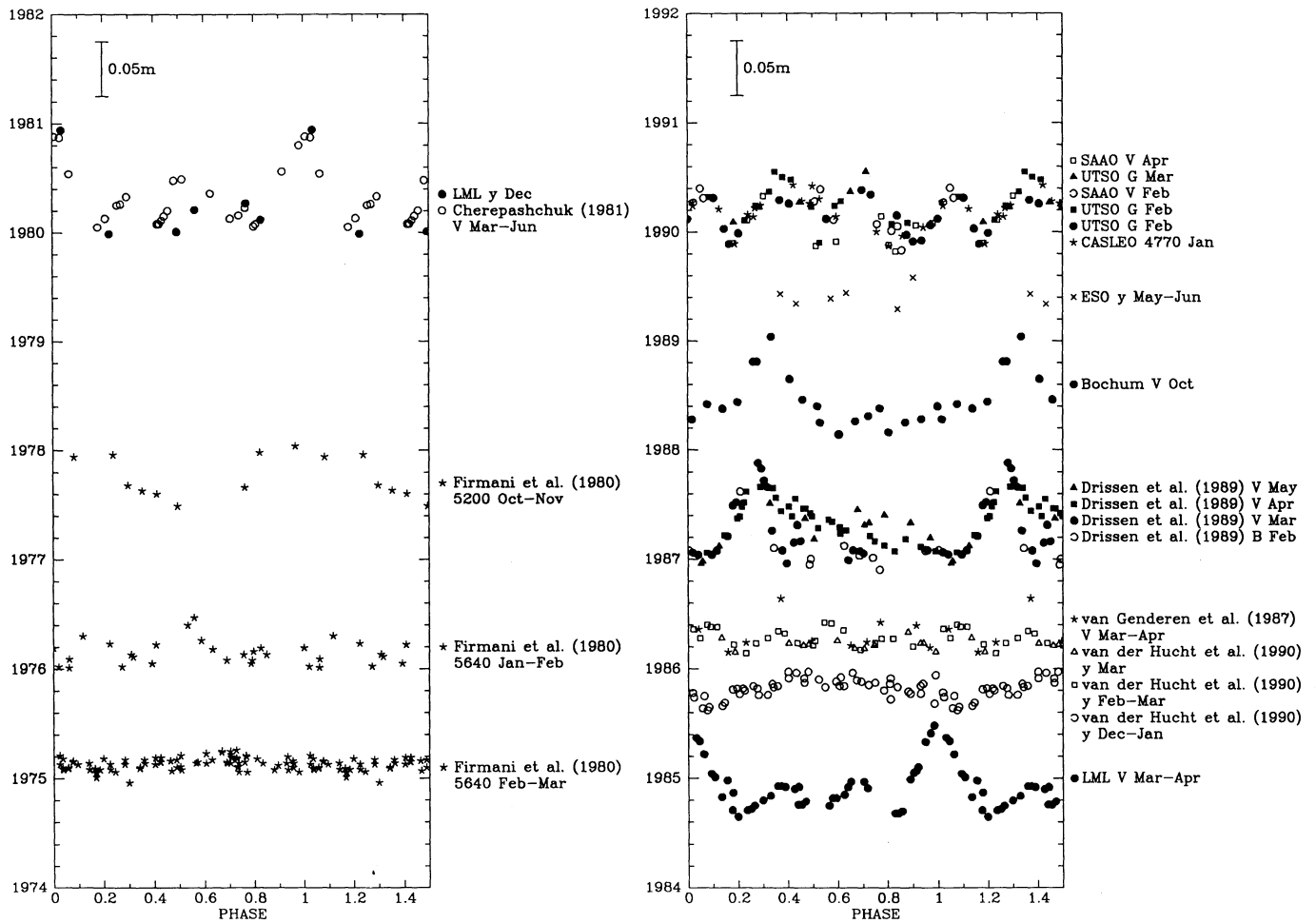

FIG. 1.—Montage of light curves of EZ CMa collected with "continuum" filters. Each curve is plotted against phase calculated with the LML ephemeris: JD 2,446,153.61 + 3.766E. Relative vertical positions of the curves are given by the year in which the observations were carried out. Data source, filter, and month of observation are indicated on the right-hand side of each curve, along with the respective symbol assigned. Superposed sets of data obtained with different filters were shifted with respect to magnitude level to match their minimum and maximum values.

this figure because they are heavily dominated by line emission, which behaves differently from the continuum; see § 3.2.) We use throughout this paper the ephemeris of Lamontage, Moffat, & Lamarre (1986, hereafter LML): JD 2,446,153.61 + 3.766*E*. From Figure 1 it is clear that the shapes of the curves, i.e., the number of maxima, and their amplitudes and phase positions, change with time. Most important to notice is that *the LML period of* 3.766 days *alway leads to a coherent light curve within each data set*. The new light curve of 1988 shows one dominant sharp maximum of amplitude 0.09 mag and a weak indication for one or two other secondary peaks. This prominent maximum shows a small shift in position by ~0.1 in phase relative to the similarly shaped light curve of Drissen et al. (1989) obtained in 1987. The last set of observations obtained in 1990 forms a completely new shape of light curve. During the 3 months of observation in 1990, the data have been collected at many different observatories using different filters. The individual data groups of 1990 do not overlap in time very well, but they show time variation which is consistent from one group to the next one. The whole light curve of 1990 evolved from two to three maxima, with a constant amplitude of 0.05 mag (see Fig. 2). A period search (using an algorithm by Press & Teukolsky 1988) among the 1990 data all together, after shifting the different sets of observations to

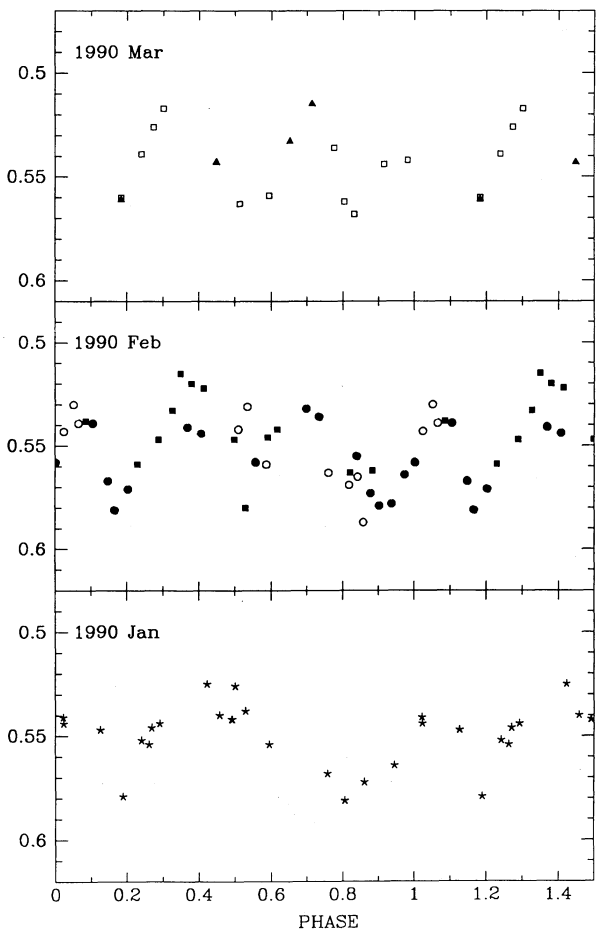

FIG. 2.—New light curves collected between 1990 January and March. Phases and symbols are as in Fig. 1. Typical error for each data point is ~0.004 mag. Evolution of the light curve is seen over a short time scale of the order of weeks.

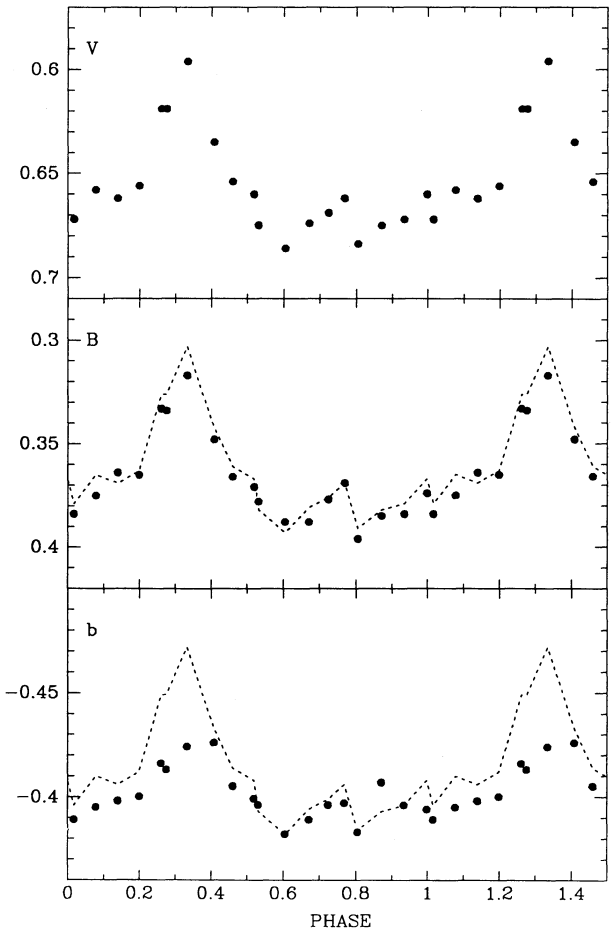

FIG. 3.—New light curves collected in 1988 simultaneously in three different filters: Johnson *V* and *B* and Strömgren *b*. Filter identification is indicated in the upper left-hand corner of each plot. Phases are as in Fig. 1. The *V* data curve (*dotted line*) is shown superposed on the *B* and *b* observations. Note the large reduction of the amplitude of variation in the *b* filter, probably due to dilution of continuum light by the emission lines which dominate the *b* filter.

the same magnitude level, reveals a period of 1.252 days [and its 1 day sampling alias $1/(1 - 1/P) \simeq 4.778$ days], along with a period of 3.762 days. This is not the first time that a short period of the order of 1 day is seen in photometry: Kuhi (1967) mentioned a photometric period of 1.01 days; Gosset & Vreux (1987) found a 1.255 day period in the photometry of LML; Balona et al. (1989) obtained a period of 1.18 days in their observations of 1988; and the appearance of four maxima within the 3.766 day period was seen in the observations of van der Hucht et al. (1990). St.-Louis et al. (1991) also found a 1 day periodicity in the equivalent widths of the absorption components of *IUE* P Cygni profiles, although a period of 3.766 days is not excluded by these data, which are spread over only ~1.3 cycles of the 3.766 day period.

3.2. *Modulation of Continuum Light versus Emission Lines*

Differences in the amplitudes of the light curves are seen when comparing data obtained simultaneously in different filters. For example, Figure 3 shows the *V*, *B*, and *b* light curves collected simultaneously in 1988. Since the light curves obtained in the different filters all show variations with the 3.766 day period, this variation is therefore caused mainly by the modulation of *continuum* light as also explained by LML

TABLE 4

PHOTOMETRY 1988 (BOCHUM 0.6 m) FILTER CHARACTERISTICS

Filter	λ_c (Å)	FWHM (Å)	Emission Lines	EW (Å)
b.....	4703	168	(N v λ4604/λ4620)	36
			He II λ4686	303
B.....	4434	970	He II λ4200	16
			He II λ4339	17
			He II λ4542	29
			N v λ4604/λ4620	36
			He II λ4686	303
			He II λ4859	35
V.....	5215	1045	(He II λ4686)	303
			He II λ4859	35
			He II λ5412	65

REFERENCES FOR EW.—Ebbets 1979; Smith & Kuhi 1981; Smith & Willis 1982; Conti, Leep, & Perry 1983; Hillier 1987; Hamann, Schmutz, & Wesslowski 1988; Schmutz, Hamann, & Wessolowski 1989; this paper.

and van der Hucht et al. (1990). Filters which include more emission-line flux have their amplitude of variation reduced due to dilution of the continuum light. One can demonstrate, for example, that for assumed constant line flux and rectangular bandpass filters, the ratio of the amplitude in *V* light to the amplitude in *b* light is given by

$$\frac{\Delta m_V}{\Delta m_b} = \frac{F_b}{F_V} \simeq \frac{1 + \mathrm{EW}_b/\mathrm{FWHM}_b}{1 + \mathrm{EW}_V/\mathrm{FWHM}_V} = 2.2 \, . \qquad (1)$$

This agrees quite well with the observations in Figure 3. Table 4 gives the list of the emission lines included in the different filters used in 1988 and their average equivalent width (EW). The filter characteristics λ_c and FWHM are also indicated. The ratio $\Delta m_V/\Delta m_B \simeq 1.1$ is again consistent with the observations of Figure 3. The less numerous data of 1989 in the *b* filter and *y* filter (with FWHM = 240 and only the strong line He II λ5412) are also in agreement with this interpretation (refer to Table 1B).

3.3 *Long-Period Search in All the Photometric Data*

In view of the dramatic but slow changes in light-curve shape, it is reasonable to search for a longer period beyond the well-established one of 3.766 days. The problem is how to characterize each curve. For the sake of simplicity, we did this by taking merely the full amplitude and standard deviation of each individual coherent light curve. Figure 4 shows the power spectrum for the long-period search in all the continuum data (i.e., curves of Fig. 1; small sets of data, less than 10 points, have been neglected, and larger samples of data have been separated into 2–3 week coherent data groups). The relatively small periods below ~50 days (i.e., above $\nu = 0.02$ day) are not considered to be real, since the light curves do not show any obvious changes on such short time scales. Relatively strong power peaks in Figure 4 are found for the long periods 101 and 651 days. A phase plot in Figure 5 of these two periods shows a relatively simple curve. However, the actual shapes of the light curves do not reveal a simple convincing progression with long-period phase. The same analysis repeated for the photometric standard deviations showed a power spectrum with similar, but less pronounced, peaks as for the amplitudes.

3.4. *Polarization Variability: Individual Curves*

The new polarimetric data of 1988 and 1990 are presented in Figure 6, along with observations from other sources already published in the literature. (We omit the isolated, much earlier

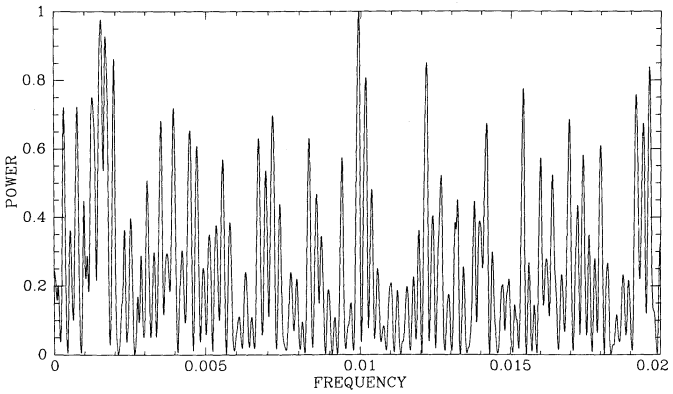

FIG. 4.—Power spectrum for the amplitude of variation of the "continuum" light curves. Two relatively strong peaks appear for $P = 101$ and 651 days.

data of Serkowski 1970 and McLean 1980, which in any case are too sparsely spread out in time to be useful here.) The phase was calculated with the ephemeris of LML. As with the photometric light curves, the shapes of the *Q* and *U* curves [with $Q = P \cos(2\theta)$ and $U = P \sin(2\theta)$] have changed considerably over the years. The changes seem to occur gradually with time and never fall near zero amplitude as does the photometry on occasion. Figure 7 shows the 1990 data separated into three groups (covering ~1 month each). The data groups obtained simultaneously at different observatories superpose each other very well. One can see a slow change of the shape of the *Q* and *U* curves with time, similar to what was observed in the 3 months' observations of 1986 presented by Drissen et al. (1989). A period search for all the 1990 polarimetric data (after shifting each data source to the same average level in *Q* and *U*) revealed a period of 3.765 days and its two (less prominent) aliases at 1.353 and 0.787 days.

Note that the 1988 October *b*-filter data show much-diminished amplitude compared with those in *y* (Fig. 8). Pre-

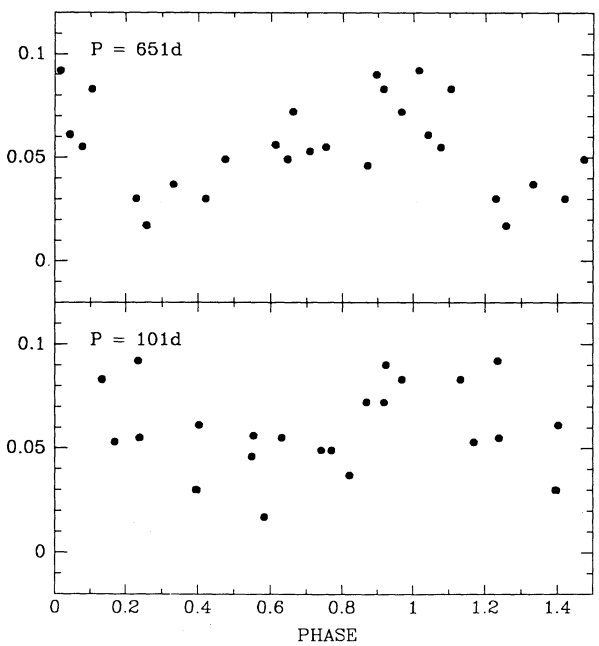

FIG. 5.—Amplitude of variation of the "continuum" light curves vs. phase for $P = 101$ and 651 days.

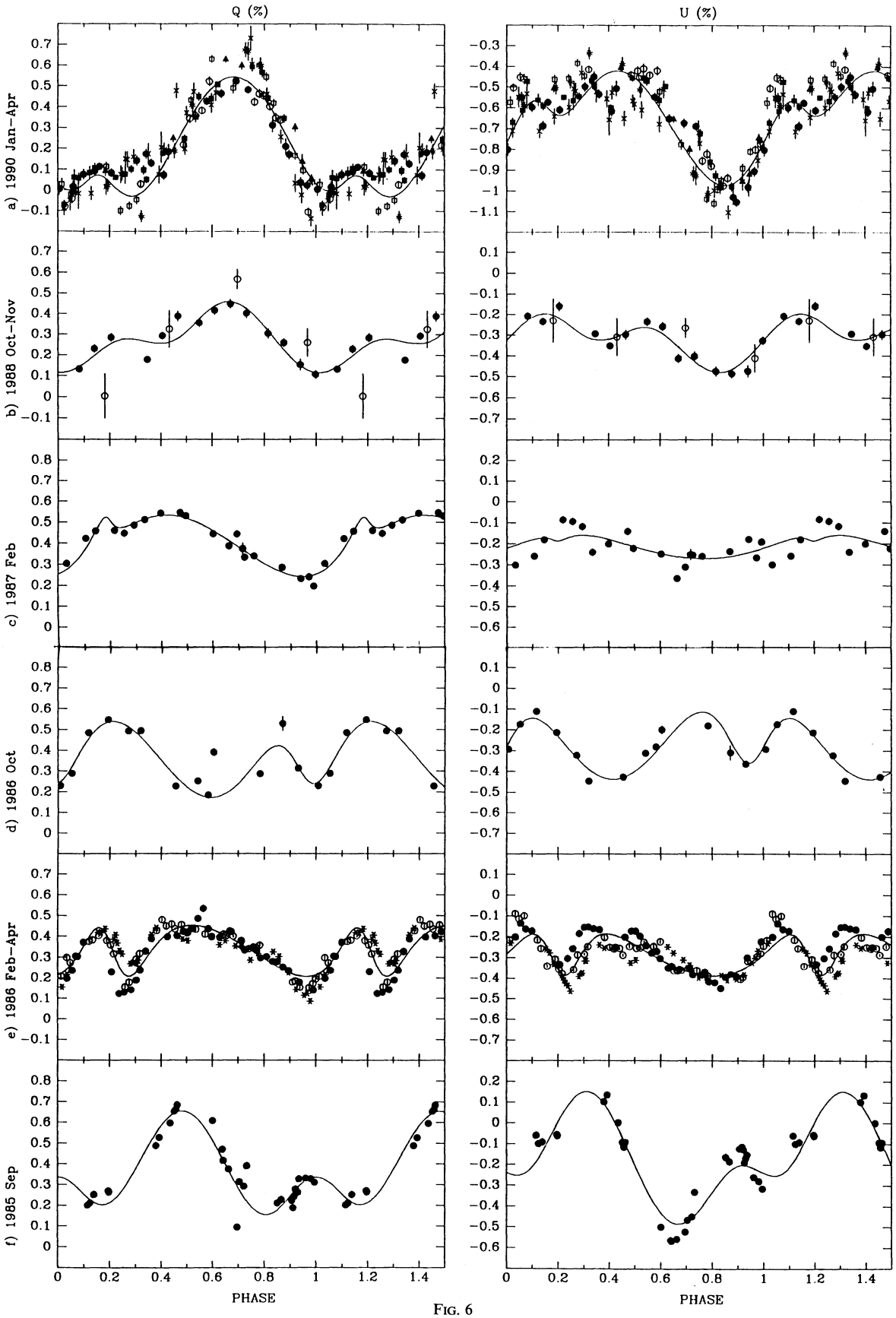

FIG. 6

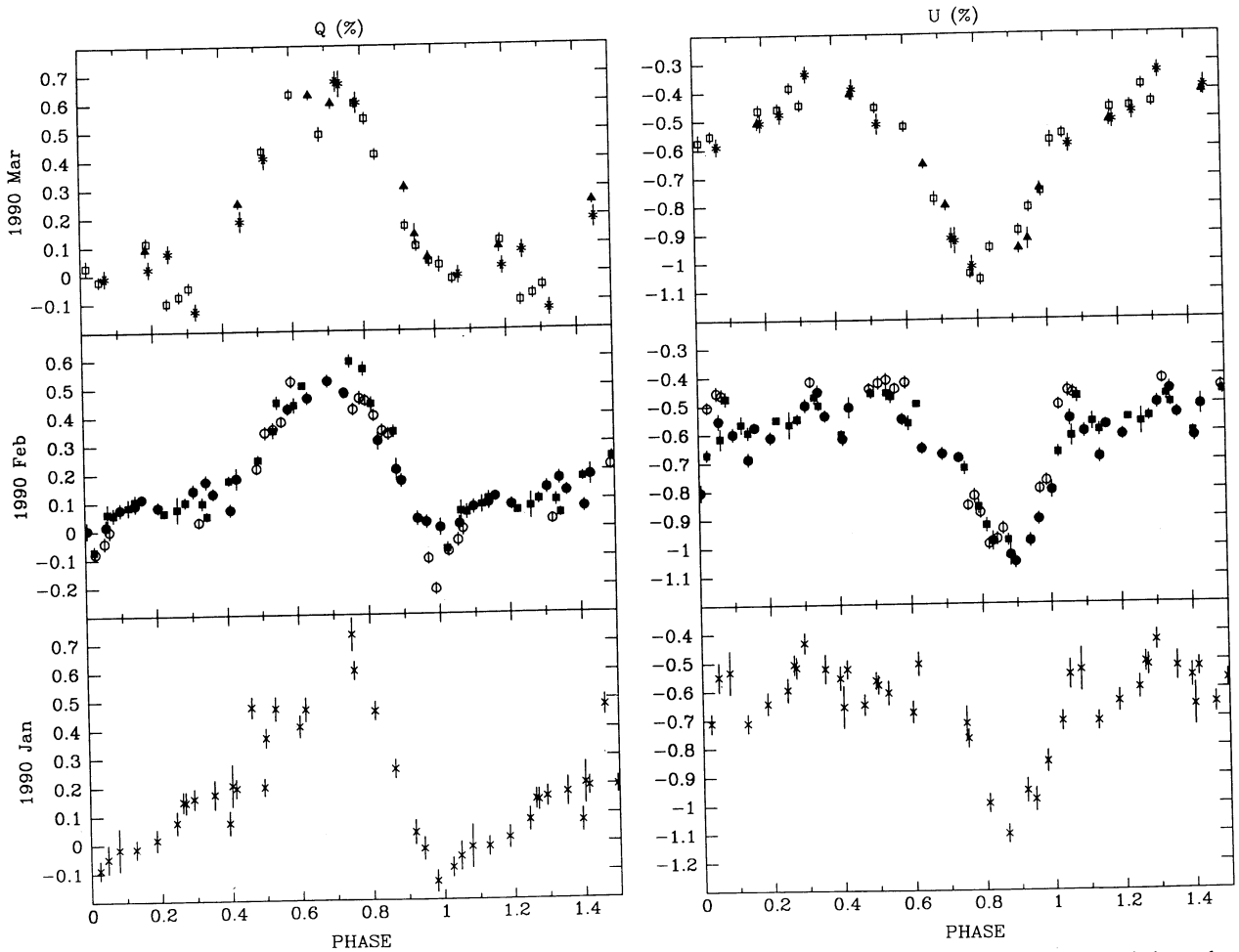

FIG. 7.—New Stokes parameters Q and U collected between 1990 January and March plotted against phase. Phases are as in Fig. 1. Symbols are the same as in Fig. 6*a*). Evolution of the polarization curves is seen over a short time scale of the order of weeks.

sumably we are seeing the same phenomenon as in the light curves, i.e., the emission lines (which dominate in the *b* filter) show little variation and are less polarized compared with the continuum. In fact, the spectropolarimetry of McLean et al. (1979) show that most of the line flux in EZ CMa is virtually unpolarized (see also § 3.10).

FIG. 6.—Stokes parameters Q and U collected since 1985 and plotted against phase. Phases are calculated as in Fig. 1. (*a*, *b*) New observations; (*c–f*) Data from Drissen et al. (1989). Different symbols refer to the observatory and filter used and to the month of observation. (*a*) (1990) *Crosses and asterisks*: CASLEO, with a continuum filter centered at 4770 Å in January and April, respectively; *filled circles, squares, and triangles*: UTSO, with a G filter at the beginning of February and at the end of February and March, respectively; *open circles and squares*: SAAO, with a *V* filter in February–March and April, respectively. (*b*) (1988) *Filled circles*: MPI, with a *y* filter in October; *open circles*: AAT, with a continuum filter centered at 5615 Å in November. (*c–f*) All data were collected with the same broad-band quasi-*B* filter ($\lambda_c = 4700$ Å, FWHM = 1800 Å). (*e*) (1986) Data are separated into three time intervals: filled circles refer to February, open circles to March, and asterisks to April. Superposed sets of data in (*a*) and (*b*) obtained with different filters have been shifted with respect to polarization level to match their minimum and maximum values. The solid line superposed on each data set is a fit to an eccentric binary model (in the case of the 1988 data in [*b*], the open circles were not considered for estimation of the best fit).

3.5. *Fits to All the Polarization Curves with an Eccentric Binary Model*

The 1986 data of Drissen et al. (1989) were relatively well fitted by the eccentric binary model of Brown et al. (1982; corrected by Simmons & Boyle 1984). Drissen et al. (1989) deduced an orbital inclination $i = 135°$, a longitude of perihelion $\lambda_p = 115°$, as well as other physical parameters, adopting an eccentricity identical to the spectroscopic value: $e = 0.34$ (Firmani et al. 1980). However, an important question arises: why do different data groups generally show such different curves if a stable eccentric binary system is to explain the observed variation? One possibility might be rapid precession effects. In an attempt to answer this question, we start as did Drissen et al. (1989), with a spherically symmetric electron distribution about the W-R star, and the following equations for the total observed linear polarization:

$$Q = Q_0 + \Delta Q \cos \Omega - \Delta U \sin \Omega ,$$
$$U = U_0 + \Delta Q \sin \Omega + \Delta U \cos \Omega , \quad (2)$$

where Ω is the angle between the major axis of the ellipse in the Q-U plane and the Q-axis (taken parallel to the cellestial north pole). The parameters Q_0 and U_0 refer to the interstellar component of polarization. Phase-dependent modulation is rep-

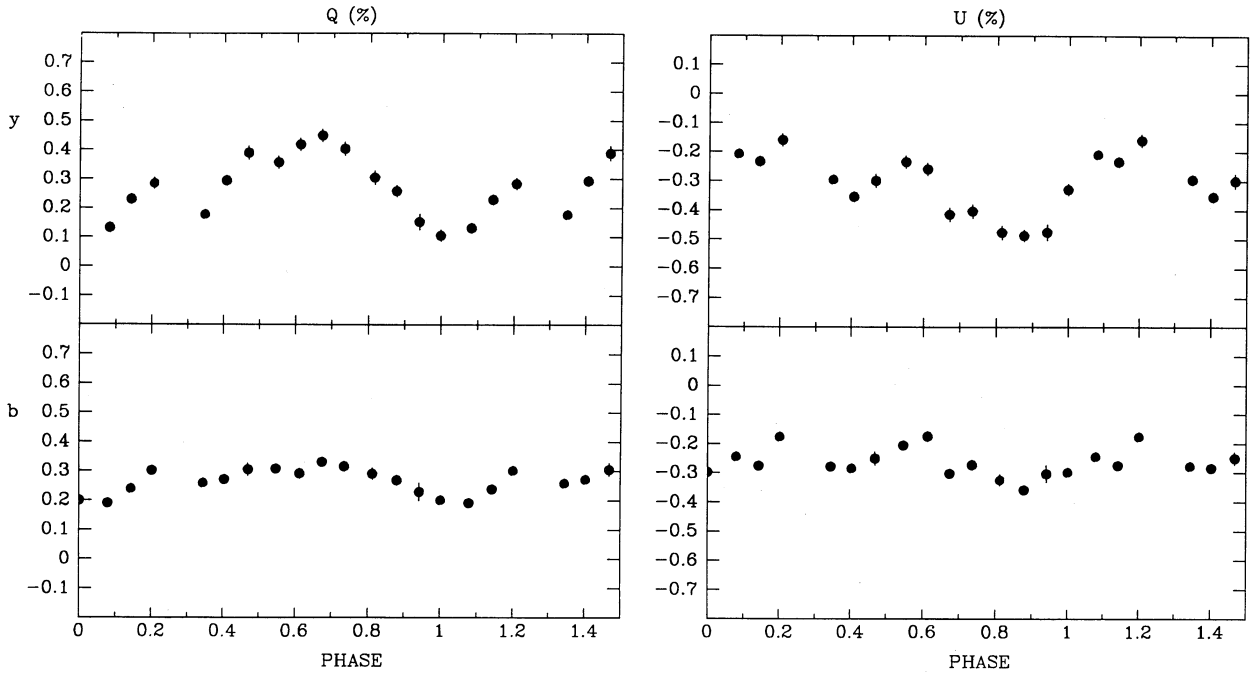

FIG. 8.—New Stokes parameters Q and U collected in 1988 simultaneously in two different filters, plotted against phase. Phases are as in Fig. 1. Note the drop in the amplitude of variation in the b filter due to dilution of the continuum light by the emission lines which dominate the b filter.

resented by

$$\Delta Q = -\tau_3[(1 + \cos^2 i)\cos(2\lambda) - \sin^2 i]\,,$$
$$\Delta U = -2\tau_3 \cos i \sin(2\lambda)\,, \quad (3)$$

where λ is the orbital longitude of the scattering region, measured in the orbital plane starting from the projection of the line of sight onto the orbital plane. The parameter τ_3 is given by (Brown, McLean, & Emslie 1978)

$$\tau_3 = \frac{3\sigma_T}{32\pi} f_c \int_0^\infty \int_0^\pi \int_0^{2\pi} n \sin^3\theta \cos(2\phi) dR\, d\theta\, d\phi\,, \quad (4)$$

where σ_T is the Thomson scattering cross section, f_c is the fraction of light coming from the companion star [$f_c = I_c/(I_{W\text{-}R} + I_c)$], and $n = n(R, \theta, \phi)$ is the electron density. The corotating spherical coordinates (R, θ, ϕ) are centered on the companion. Brown et al. (1982) found, for an eccentric orbit, in the specific case of a *localized* electron envelope containing N electrons relatively close to the star compared to the semimajor orbital axis a:

$$\tau_3 = \tau_*\left(\frac{a}{r}\right)^2 = \tau_*\left[\frac{1 + e\cos(\lambda - \lambda_p)}{1 - e^2}\right]^2\,, \quad (5)$$

where τ_* is related to the electron density around the W-R star ($\tau_* = 3\sigma_T N/32\pi a^2$) and r is the time-dependent separation between the stars. The parameter λ_p is the longitude of periastron. The above equations are identical to what Drissen et al (1989) used to fit the 1986 polarimetric data of EZ CMa.

To improve the model, we take into account here the *extended* envelopes (not localized close to the star) of W-R stars. Numerical values of τ_3 in equation (4) were calculated by St.-Louis et al. (1988) for a realistically extended W-R electron envelope and different values of a. They obtained $\tau_3 \propto (a/r)I$ (i.e., eq. [5] of St.-Louis et al. 1988, in which a has been replaced by a variable r for an eccentric binary orbit and the new mean orbital separation a is used for normalization). The function I is plotted against r/R_* in Figures 9 and 10 of St.-Louis et al. (1988) for different values of β ($\lesssim 1$), the power index in the wind velocity law, and ϵ, the relative distance in the wind where the optically thin, central point source approximation begins. For small r, $I \propto (r/a)^x$ is an appropriate approximation in a limited range of r/a, in which x is a small constant. This leads to $\tau_3 \propto (a/r)^{1-x}$. Therefore, for an orbit of moderate eccentricity in which a unique value of x is likely to apply, and for a realistically extended W-R envelope, we use equation (5) for τ_3, where we replace the exponent 2 by a free parameter γ. For wide separations γ reaches unity; otherwise $\gamma < 1$.

In Figure 6 the full-line curves are the best fits obtained using the eccentric model with γ a free fitted parameter. Table 5 gives the best set of parameters obtained for each curve. From Table 5 there is a tendency for some of the basic parameters to lie in a narrow range, within the errors. In particular, the mean orbital eccentricity $e = 0.39 \pm 0.02$ is close to the spectroscopic value for the radial velocity orbit of Firmani et al. (1980): $e = 0.34 \pm 0.08$. Also, the mean orbital inclination $i = 114° \pm 3°$ is equivalent to $i = 180° - 114° = 66° \pm 3°$ in the context of velocity orbits. For γ there may be real deviations from one group to the other. In a binary model, epoch changes could result due to variations (of unknown origin) in the electron distribution around the W-R star which could reflect themselves through the parameter γ.

Unfortunately, there are still not enough polarimetric data to make a viable search for a long precession period.

3.6 *Circular Polarization*

The new circular polarization data collected in 1990 are presented in Figure 9. No phase-locked variations are seen in the new data group, as in 1987 (see Drissen et al. 1989). The

TABLE 5

PARAMETERS FROM THE ECCENTRIC BINARY MODEL

Data Group[a]	Mean JD −2,440,000.0	e	λ_p	i	Ω	τ_*	γ	T_0 −2,446,000.0
1990	7943.932	0.54 ± 0.06	48° ± 14°	126° ± 5°	291° ± 19°	0.12 ± 0.03	−2.6 ± 0.6	498.6 ± 0.1
1988	7446.379	0.54 ± 0.41	355 ± 13	115 ± 26	55 ± 40	0.07 ± 0.05	−4.0 ± 2.7	499.5 ± 0.2
1987	6840.356	0.73 ± 0.20	27 ± 19	99 ± 6	177 ± 20	0.12 ± 0.04	−1.8 ± 1.4	500.8 ± 0.2
1986 Oct	6722.512	0.36 ± 0.12	349 ± 23	117 ± 20	46 ± 49	0.14 ± 0.07	−1.6 ± 1.4	499.9 ± 0.2
1986 Feb–Apr	6507.114	0.37 ± 0.02	317 ± 7	112 ± 4	31 ± 10	0.11 ± 0.01	−0.1 ± 0.3	500.8 ± 0.1
1985	6367.509	0.49 ± 0.12	348 ± 12	122 ± 11	143 ± 30	0.12 ± 0.05	−3.6 ± 1.0	500.1 ± 0.1
Weighted mean	...	0.39 ± 0.02	344 ± 5	114 ± 3	44 ± 8	0.11 ± 0.01	−0.9 ± 0.8	499.9 ± 0.1
σ	...	0.06	31°	9°	73°	0.01	0.8	0.9

[a] 1985–1987: Drissen et al. 1989; 1988–1990: this paper.

standard deviation is still very low. We find the same average circular polarization as in 1987: $\bar{V} = 0.015\% \pm 0.002\%$ in 1987 and $0.014\% \pm 0.003\%$ in 1990 (February and April). There is some indication for a higher average value of V during 1990 April. The small, and almost constant, level of circular polarization may be of interstellar origin (as proposed by Drissen et al. 1989) and/or of instrumental origin (as suggested by the small shift between the data of 1990 February and April). These results provide evidence that EZ CMa does not show activity related to a strong magnetic field either localized in loops, uniformly spread far out in the wind, or associated with a compact companion. Observations at radio and millimeter wavelengths of EZ CMa also show no evidence for nonthermal emission (e.g., Leitherer & Robert 1991).

3.7. *Spectroscopic Variability: Profiles*

The wavelength range selected for the spectroscopic observations includes three strong emission lines: He II λ5412, C IV λ5807, and He I λ5876. Peculiarities prevail in these lines. The red wing of He II λ5412 (with laboratory wavelength 5411.52; Moore 1945) is more extended either due to some unidentified, weaker emission lines (Smith & Kuhi 1981) and/or due to electron scattering (Hillier 1984). C IV λ5807 consists of two blended lines at 5801.51 and 5812.14 Å of relative strength 4:3 (Moore 1945). He I λ5876 is also a blended triplet with emissions of almost equal strength at 5875.618, 5875.650, and 5875.989 Å. Models of Hillier (1987) and Hamann, Schmutz, & Wessolowski (1988) show a P Cygni profile for He I λ5876 line where the absorption part of the profile overlaps with C IV λ5807 line. Strong interstellar absorption lines due to Na I λ5890/λ5896 are superposed on He I λ5876.

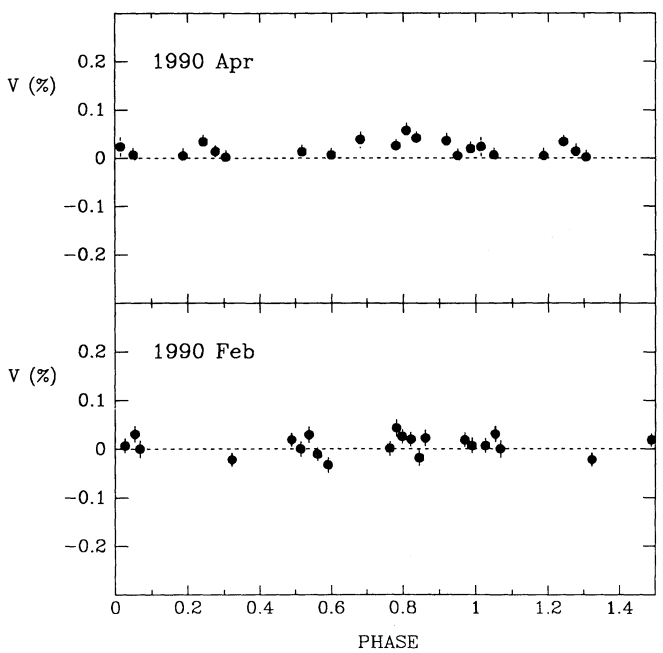

FIG. 9.—Circular polarization data collected in 1990 plotted against phase (calculated as in Fig. 1).

Figure 10 presents the mean profiles of the three lines for each night of observation (for the ESO run—1989 May–June—only one spectrum was collected per night; refer to Table 3 for details of the observing runs). Comparison of the mean spectra from night to night reveals global profile variations in the three lines. (We will discuss at the end of this section the relatively small variations seen in spectra collected during the same night.) The changes of the profile shapes can be roughly described as the superposition of a relatively narrow emission component on a broad wind profile. To illustrate the profile variations further, we plot in Figure 11 the difference spectra for the essentially unblended He II line. These spectra represent the nightly mean differences between spectra of Figure 10 and the *overall* mean spectrum calculated from the mean for all nights from 1988 to 1990 and smoothed with a 5 pixel boxcar. The overall mean spectrum (relatively smooth!) is present in Figure 11 superposed on the difference spectra of the 1989 February observing run. No wavelength shifts were performed on the spectra before we applied the subtraction. (In the next section we discuss the small-amplitude radial velocity variations.)

Profile variations in EZ CMa were also seen before in a large sample of optical lines (e.g., Ebbets 1979; Firmani et al. 1980; Underhill & Yang 1991). It was found that the He II Pickering lines all varied in the same fashion, while different ions behaved quite differently. Correlations among the structures seen in the top parts of the three line profiles studied here are not obvious, possibly due to the fact that C IV λ5807 and He I λ5876 are blended and that absorption lines of interstellar Na I λ5890/λ5896 and telluric H_2O mask a large portion of the He I λ5876 profile. According to Figures 10 and 11, it is not obvious either that profile changes clearly repeat themselves from one epoch to another over a period of 3.766 days as was the case for Firmani et al. (1980). To verify the periodicity in the profile morphology, we calculated the skewness $\beta_1^{1/2}$ for the relatively simple unblended line He II λ5412. This parameter is a dimensionless measurement of the line asymmetry; it is given by the ratio of the third and (3/2 power of the) second central

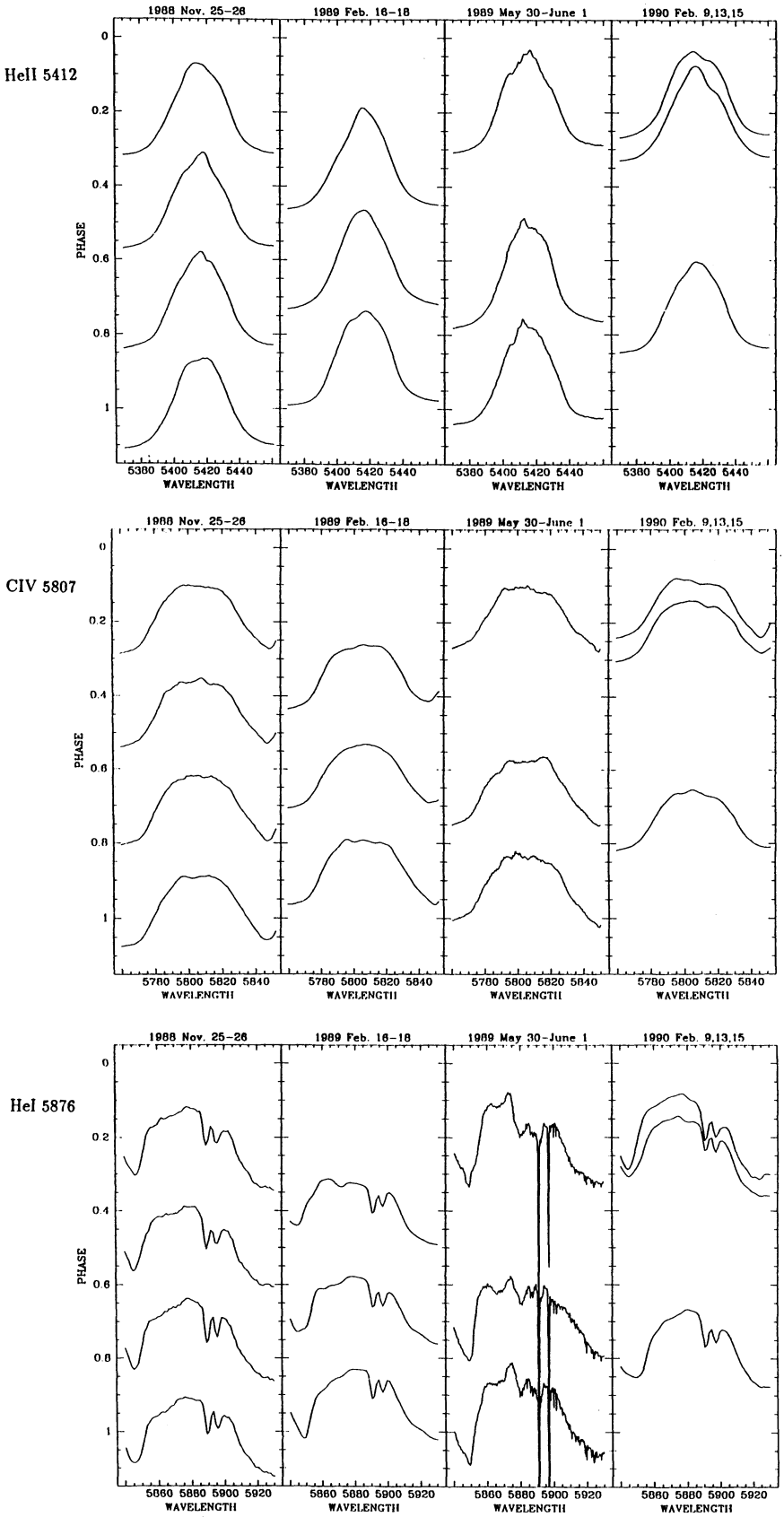

FIG. 10

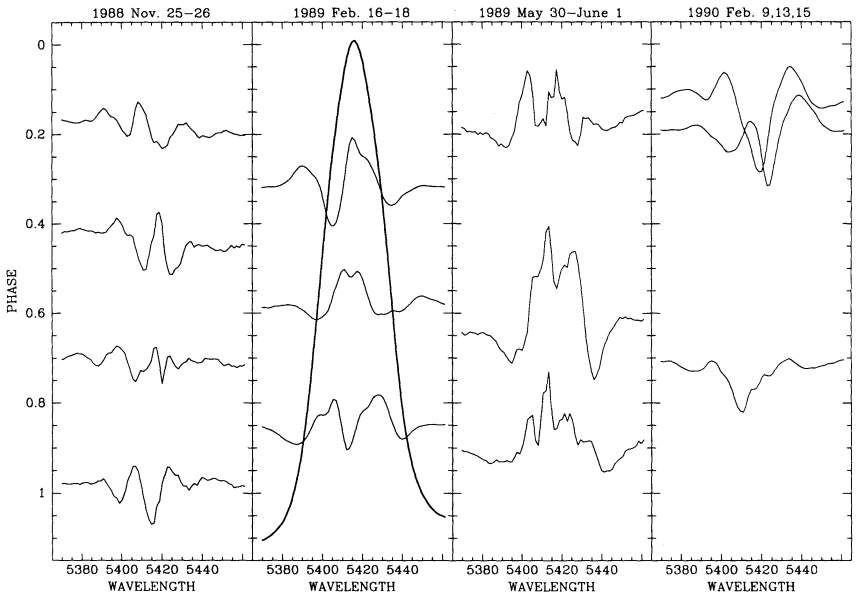

FIG. 11.—Differences from the overall mean of the spectra in Fig. 10 for He II λ5412. The overall mean is the average of the nightly mean spectra collected between 1988 and 1990. It is superposed on the differences for the second spectroscopic run in 1989 February. The differences are multiplied by a factor of 3 compared with the overall mean.

moments of the line:

$$\beta_1^{1/2} = \mu_3/\mu_2^{3/2}\,, \quad \mu_n = \sum_i (\lambda_i - \bar{\lambda})^n I_i \Big/ \sum_i I_i\,, \quad \bar{\lambda} = \sum_i \lambda_i I_i \Big/ \sum_i I_i\,, \tag{6}$$

where λ_i is the wavelength corresponding to the ith intensity line level, I_i, starting at 10% of the maximum intensity in the line. The skewness $\beta_1^{1/2}$ is shown plotted against phase in Figure 12; it shows a weak periodic dependence (which is confirmed by the period search algorithm of Press & Teukolsky 1988). Shifts in $\beta_1^{1/2}$ between epochs may have occurred (as seen for the photometric and polarimetric data), which complicate the coherent periodic behavior of the profile changes. Unfortunately, phase coverage is too poor to allow any conclusion about periodic profile morphology for each run separately.

We have also looked for radially expanding condensations of wind material, i.e., blobs, in the wind of EZ CMa. Blobs are not unusual for W-R stars (e.g., Moffat et al. 1988; Robert 1992; Moffat & Robert 1992). Figure 13 presents time sequences of spectra. Time coverage only reached ~4 hr for the best nights. As one can see, the amplitude of the root mean square (rms), calculated from the square root of the variance with respect to the average spectrum for each run, increases in the lines. This indicates that real, short time-scale variations are occurring in the wind of EZ CMa. The variations are seen in the three lines; some nights they are strongest in either the blue or the red side of He II λ5412 or in the region between C IV λ5807 and He I λ5876 (which corresponds to the absorption part of the He I λ5876 P Cygni profile).

Figure 14 shows a few examples of time sequences for the difference spectra of He II λ5412. These are the differences of the first spectrum collected for the night with other spectra collected the same night. In Figure 14 we can see many bumps in the line which are slowly evolving, in position and amplitude, with time. Most of these structures show outward acceleration, i.e., the blue or red bumps become more blueshifted or redshifted, respectively, with time. Some of the bumps seem to remain at the same wavelength position during a night, although the observing interval may be too short to reveal any significant motion. In general, the spectroscopic bumps of EZ CMa show similar behavior to the blobs seen in other W-R stars; they probably have the same origin, maybe instabilities in a radiatively driven wind (e.g., Lucy 1982; Owocki, Castor, & Rybicki 1988). The highest radial velocity measured for the blobs of EZ CMa is ~1800 km s^{-1} (Fig. 14; one of the red bumps seen on 1990 February 13). This coincides well with the terminal ("black") velocity measured by Prinja, Barlow, &

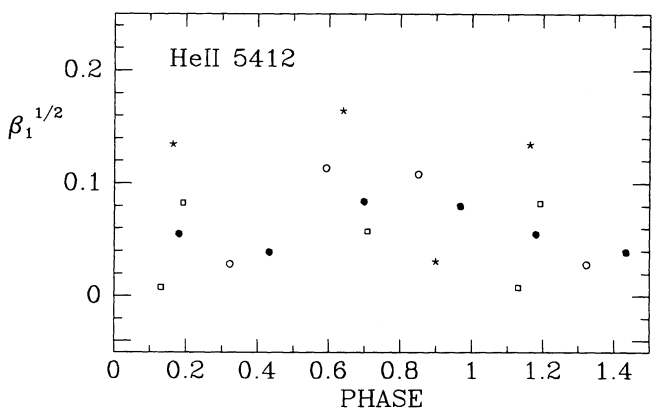

FIG. 12.—Skewness vs. phase for the nightly averaged He II λ5412 profile. Phases are as in Fig. 1. Symbols are as follows: *filled circles*, AAT, 1988 November; *open circles*, OMM, 1989 February; *asterisks*, ESO, 1989 May–June; *open squares*, OMM, 1990 February.

FIG. 10.—Mean profiles for each night of spectroscopic observations for the emission lines He II λ5412, C IV λ5807, and He I λ5876. The profiles are vertically ordered according to phase (calculated as in Fig. 1). Four panels are presented for each line to separate the four spectroscopic runs: AAT in 1988 November, OMM in 1989 February, and 1990 February, and ESO in 1990 May–June. Periodic changes of the profiles are not evident.

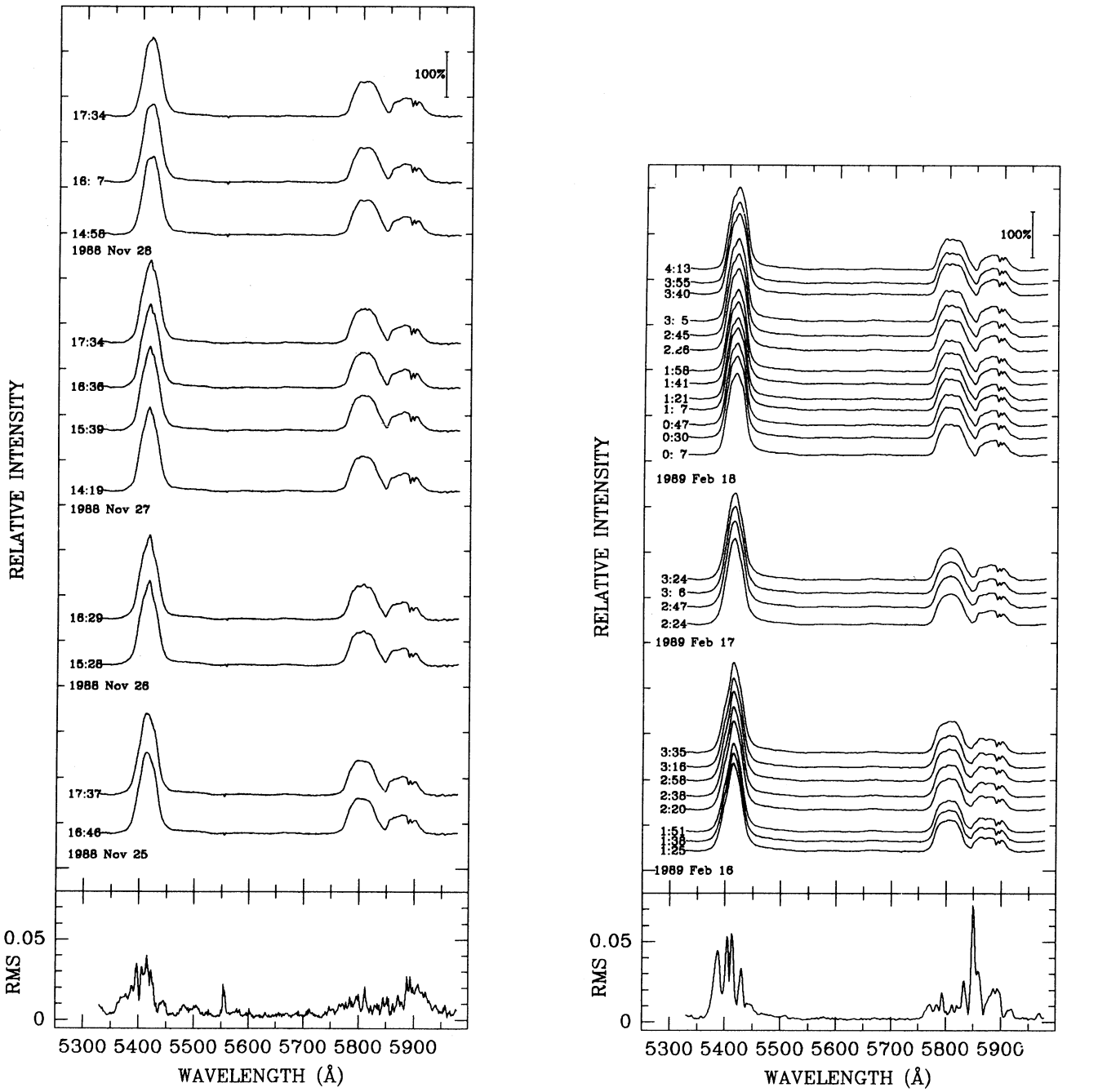

FIG. 13.—Time series of the spectra. Day and universal time are given for each observation and increase from bottom to top. The rms curves, presented in the lower panel, were calculated with respect to the mean spectrum for each run.

Howarth (1990; $v_\infty \simeq 1720$ km s^{-1}). Further details of the blobs of EZ CMa (and also the global profile changes) will require spectra with more complete time coverage.

3.8. *Radial Velocities*

Radial velocities were obtained from the mean spectra of each night by measuring the line center at different intensity levels in the lines. Two different techniques were developed to calculate the line center: one of them consists of measuring the line bisector (i.e., the average wavelength on each side of the line at the desired intensity level); the other method consists of dividing the integrated flux into two equal parts on each side of the line center above a certain level. The latter method will centainly be more sensitive to the structure seen at the peak of the line, especially when the line center is measured at a higher intensity level. Radial velocities obtained for the three lines with these techniques are listed in Tables 6A–6C.

Radial velocities measured at a low intensity level in He II λ5412 show a noisy, but significant, phase dependency with the 3.766 day period. A period search carried out in these radial velocity data confirmed this periodicity. Figure 15 shows, plotted against the LML phase calculated with the 3.766 days

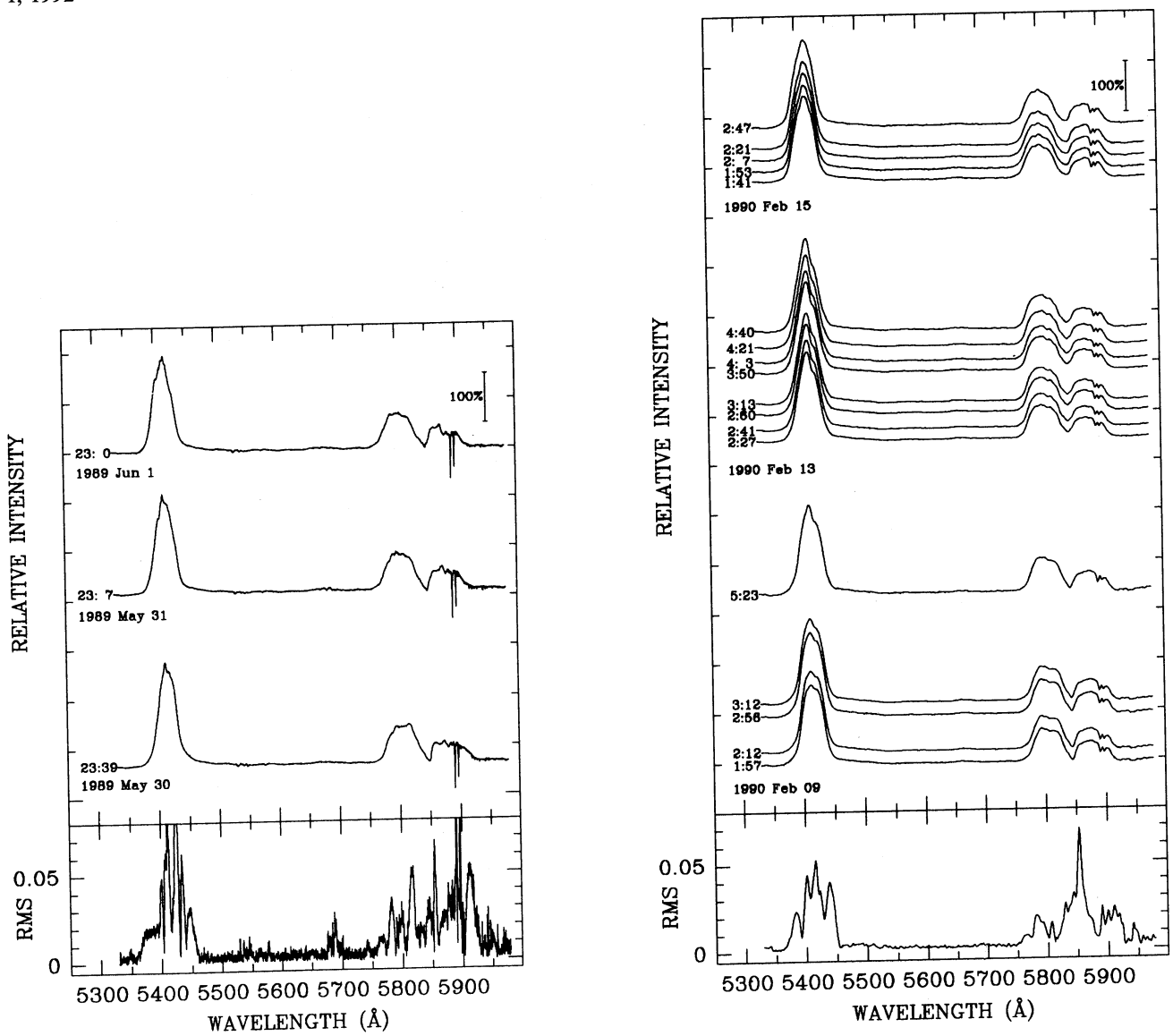

FIG. 13—*Continued*

period, the radial velocity data obtained by extracting the line center with the bisector method at a low intensity level (10% of the maximum intensity). No significant phase dependence can be seen if the line center is measured higher in the line. The orbital parameters for the best fit shown in Figure 15 with the eccentricity forced to be equal to the value obtained by Firmani et al. (1980), $e = 0.34$, and compatible with the polarimetry, are presented in Table 7. The systemic velocity, γ, is higher than that previously found for He II λ5412 and other He II lines (i.e., $\simeq 150$ km s^{-1} from Wilson 1948; Ebbets 1979; Firmani et al. 1980; Niemela & Méndez 1982; LML; Hillier 1987; Underhill & Yang 1991). The amplitude of the radial velocity data, K, may be larger than that found on average in previous studies (e.g., Firmani et al. 1980 calculated $K = 25 \pm 9$ km s^{-1} for He II λ4686).

Phase variations of C IV λ5807 were found for radial velocity data measured at the top of the line (90% of the maximum intensity) with the half-flux method (Fig. 15). The periodicity was confirmed by the period search program. The orbital parameters obtained for the best radial velocity fit are presented in Table 7. Radial velocities measured lower in the line or with the bisector techniques showed no significant phase dependency. This may be due to the fact that this line overlaps with the absorption part of the P Cygni profile of He I λ5876 or because it is a blended doublet.

The most convincing phase-dependent radial velocity variation was obtained in the case of He I λ5976. Maximum amplitude of the variation was found when the line center is measured at 30% of maximum intensity with the half-flux method. Table 7 lists the orbital parameters deduced for the best fit in Figure 15.

For the three lines we obtain rather discordant values of ω, T_0, and E_0. This is inconsistent with a *simple* binary model for EZ CMa as noted previously by Firmani et al. (1980). It is probable that profile variations affect the radial velocity changes. Possibly, global perturbations may be more evident for some lines than for others. In general, weaker lines of higher ionization tend to be seen at lower levels in the W-R wind

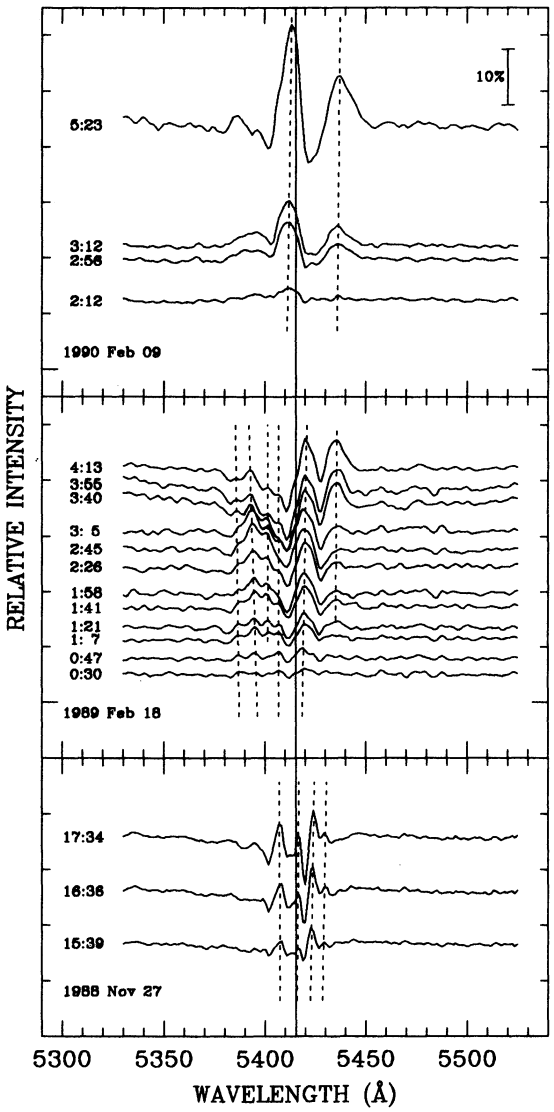

FIG. 14.—Time series of differences of spectra in Fig. 13. The differences were obtained by subtracting the first spectrum collected for each night. Only three nights with a time coverage larger than 2–3 hr are presented here. The Universal Time is given for each difference. The vertical line indicates the geometrical line center of the overall mean. Dotted lines show the slow radially outward acceleration of the blobs.

(Hillier 1985, 1987; Shylaja 1986). The fact that for He II λ5412 we find periodic variations of the profile asymmetry (compare Figs. 12 and 15: $\beta_1^{1/2}$ varies in phase with the radial velocity) even suggests that the observed radial velocity could be totally generated by them. In addition, the radial velocity data are spread over a 2 year interval during which epoch-dependent spectral changes may have occurred, as seen in photometry and polarimetry. Niemela & Méndez (1982) have already pointed out some changes of the radial velocity amplitude of lines of N IV which confirmed this idea. The hypothesis of radial velocity variations in EZ CMa *strictly* due to systematic motion of the lines, as in a binary system, is not clearly demonstrated here. Nevertheless, some component of binary-type regularity cannot be excluded.

3.9. *Equivalent Widths*

Equivalent widths for the three lines are plotted against phase (calculated with the LML ephemeris) in Figure 16. They were measured in the wavelength range 5355–5548 Å for He II λ5412, 5750–5846 Å for C IV λ5807, and 5846–5920 Å for He I λ5876 and are listed in Table 8.

There emerges no clear phase dependence of the equivalent widths, although a period search revealed a weak peak around the 3.766 day period for He II λ5412. Periodic variations and epoch changes of line flux or equivalent width have been observed before for this line and other Pickering He II lines (Firmani et al. 1980; Singh 1984; Shylaja 1986). Again, epoch-dependent variations may be responsible for drowning out any

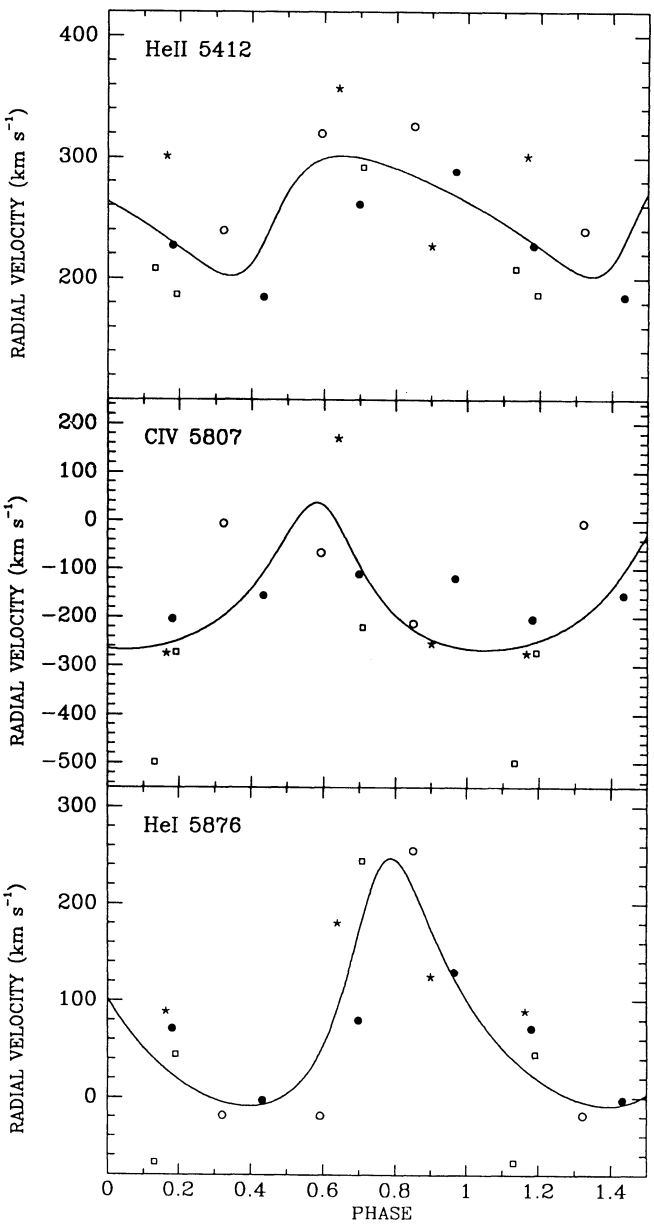

FIG. 15.—Radial velocities vs. phase for the emission lines He II λ5412, C IV λ5807, and He I λ5876. Phases are as in Fig. 1. Symbols are the same as in Fig. 12. The solid lines are best fits to a binary model with eccentricity fixed to 0.34.

TABLE 6A

RADIAL VELOCITIES FOR He II λ5412

OBSERVATORY	JD −2,447,000	φ	BISECTOR 10% (km s^{-1})	BISECTOR 50% (km s^{-1})	BISECTOR 90% (km s^{-1})	HALF-FLUX 10% (km s^{-1})	HALF-FLUX 50% (km s^{-1})	HALF-FLUX 90% (km s^{-1})
AAT	491.219	0.180	227	179	104	174	172	94
	492.169	0.433	185	165	214	169	166	245
	493.167	0.698	261	176	161	189	190	172
	494.181	0.967	289	204	170	200	194	229
OMM	574.607	0.323	239	177	199	190	220	176
	575.624	0.593	320	196	144	190	169	158
	576.593	0.850	326	182	196	198	204	253
ESO	677.482	0.639	357	196	167	198	202	84
	678.460	0.899	227	199	145	185	175	101
	679.455	0.163	301	176	219	178	153	200
OMM	931.656	0.131	208	204	77	193	174	54
	935.651	0.192	187	230	128	216	180	147
	937.596	0.708	292	193	235	206	217	222
Mean	...	...	263	190	166	191	186	164
σ	...	...	56	17	47	13	21	65

NOTE.—Phases, φ, are as in Table 1A.

TABLE 6B

RADIAL VELOCITIES FOR C IV λ5807

OBSERVATORY	JD −2,447,000	φ	BISECTOR 30% (km s^{-1})	BISECTOR 50% (km s^{-1})	BISECTOR 90% (km s^{-1})	HALF-FLUX 30% (km s^{-1})	HALF-FLUX 50% (km s^{-1})	HALF-FLUX 90% (km s^{-1})
AAT	491.219	0.180	−21	−113	−113	−113	−131	−204
	492.169	0.433	−31	−101	−127	−110	−134	−156
	493.167	0.698	−12	−107	−143	−99	−118	−111
	494.181	0.967	−21	−88	−114	−89	−105	−120
OMM	574.607	0.323	−90	−145	−93	−134	−129	−6
	575.624	0.593	−44	−112	−99	−101	−104	−66
	576.593	0.850	−27	−101	−93	−107	−125	−213
ESO	677.482	0.639	−12	−117	−26	−73	−52	170
	678.460	0.899	−66	−137	−199	−115	−115	−254
	679.455	0.163	−16	−91	−165	−94	−110	−274
OMM	931.656	0.131	−100	−126	−267	−145	−170	−499
	935.651	0.192	−3	−101	−158	−115	−141	−272
	937.596	0.708	−87	−103	−278	−120	−138	−221
Mean	...	...	−41	−111	−144	−109	−121	−171
σ	...	...	34	17	71	19	27	159

NOTE.—Phases, φ, are as in Table 1A.

TABLE 6C

RADIAL VELOCITIES FOR He I λ5876

OBSERVATORY	JD −2,447,000	φ	BISECTOR 30% (km s^{-1})	BISECTOR 50% (km s^{-1})	HALF FLUX 30% (km s^{-1})	HALF FLUX 50% (km s^{-1})
AAT	491.219	0.180	239	179	71	9
	492.169	0.433	142	139	−3	−70
	493.167	0.698	230	153	80	40
	494.181	0.967	267	196	129	87
OMM	574.607	0.323	133	127	−18	−97
	575.624	0.593	136	127	−19	−100
	576.593	0.850	−189	262	255	238
ESO	677.482	0.639	455	278	180	176
	678.460	0.899	259	193	125	156
	679.455	0.163	270	215	89	150
OMM	931.656	0.131	159	139	−67	−142
	935.651	0.192	160	197	45	−29
	937.596	0.708	390	341	244	181
Mean	...	...	204	196	85	46
σ	...	...	154	65	100	127

NOTE.—Phases, φ, are as in Table 1A.

TABLE 7

RADIAL VELOCITY ORBITS WITH $P = 3.766$ days AND $e = 0.34$

Parameter	He II λ5412	C IV λ5807	He I λ5876
γ (km s^{-1})	259 ± 3	−166 ± 5	81 ± 2
K_{W-R} (km s^{-1})	50 ± 20	152 ± 52	128 ± 4
ω	244° ± 66°	8° ± 48°	331° ± 39°
T_0 (JD)[a]	676.7 ± 0.5	677.3 ± 0.4	677.9 ± 0.2
E_0 (JD)[a]	492.3 ± 0.6	491.9 ± 0.4	492.9 ± 0.3

[a] JD −2,447,000.0.

phase dependence for He II λ5412 in our generally small data groups. For C IV λ5807 and He I λ5876, we find no short-term periodicity but find strong changes in the level at different epochs. However, we suspect that variations in C IV λ5807 and He I λ5876 may be partially due to variable atmospheric H_2O absorption at these wavelengths (even though we applied first-order corrections for this effect in the OMM spectra taken at high air mass).

3.10. *Spectropolarimetry*

Figure 17 presents the mean of each night for $P(\lambda)$, $Q(\lambda)$, $U(\lambda)$, and $F(\lambda)$ in 8 Å bins. The figure clearly indicates that the polarization degree drops in the emission lines compared with the continuum. This result is similar to that first found by McLean et al. (1979) for this star.

The mean continuum polarization is plotted against phase in Figure 6. Compared with the y-band data obtained 6 weeks earlier, some changes have occurred, but there still remains some similarity.

Inspection of the line polarization parameters in Figure 17 shows dramatic changes from night to night. No detectable polarization variations in the lines were seen for the spectra collected during the same night. The night-to-night changes appear to be similar in each of the three lines He II λ5412, C IV λ5807, and He I λ5876, although they are strongest and clearest in He II λ5412. As a particular example, we draw attention to the first and third nights (when the continuum polarization differs most; see Fig. 17): within the noise level for He II λ5412, the maximum in $Q(\lambda)$ shifts by ~30 Å and the amplitude of Q across the line is much larger on the first night, when the continuum polarization is much lower. On the other hand, very little change occurs in $U(\lambda)$ across the line, since the continuum polarization level in U remains nearly constant.

The above changes can also be studied by tracing Q versus U across the strongest line He II λ5412 (Fig. 18). Here we see a closed blue-to-red loop that is traced out in anticlockwise direction during the first night and in clockwise direction on the 3 following nights. This behavior contrasts with that reported by Schulte-Ladbeck et al. (1990), in which they saw only clockwise motion, even though the amplitudes of the Q-U loops are all similar. Furthermore, there is a progression of shapes in the Q-U plane, for elongated at $\varphi = 0.967$ and 0.181 to rounder at $\varphi = 0.433$ and especially $\varphi = 0.698$. It is interesting to note that the He II λ5412 profiles show maximum skewness at $\varphi \simeq 0.70$, corresponding to the round Q-U loop.

TABLE 8

EQUIVALENT WIDTHS

Observatory	JD −2,447,000	φ	He II λ5412 (Å)	C IV λ5807 (Å)	He I λ5876 (Å)
AAT	491.219	0.180	71.9	40.4	19.8
	492.169	0.433	72.1	39.4	18.2
	493.167	0.698	70.8	40.3	19.9
	494.181	0.967	70.0	40.2	20.1
OMM	574.607	0.323	73.0	35.4	16.5
	575.624	0.593	75.0	34.9	16.2
	576.593	0.850	72.0	35.2	16.0
ESO	677.482	0.639	76.6	37.8	19.3
	678.460	0.899	73.0	36.8	18.2
	679.455	0.163	71.1	37.7	19.4
OMM	931.656	0.131	73.0	33.0	17.7
	935.651	0.192	71.9	33.9	18.6
	937.596	0.708	69.6	32.0	16.9
Mean	...	...	72.3	36.7	18.2
σ	...	...	1.9	2.9	1.5

NOTE.—Phases, φ, are as in Table 1A.

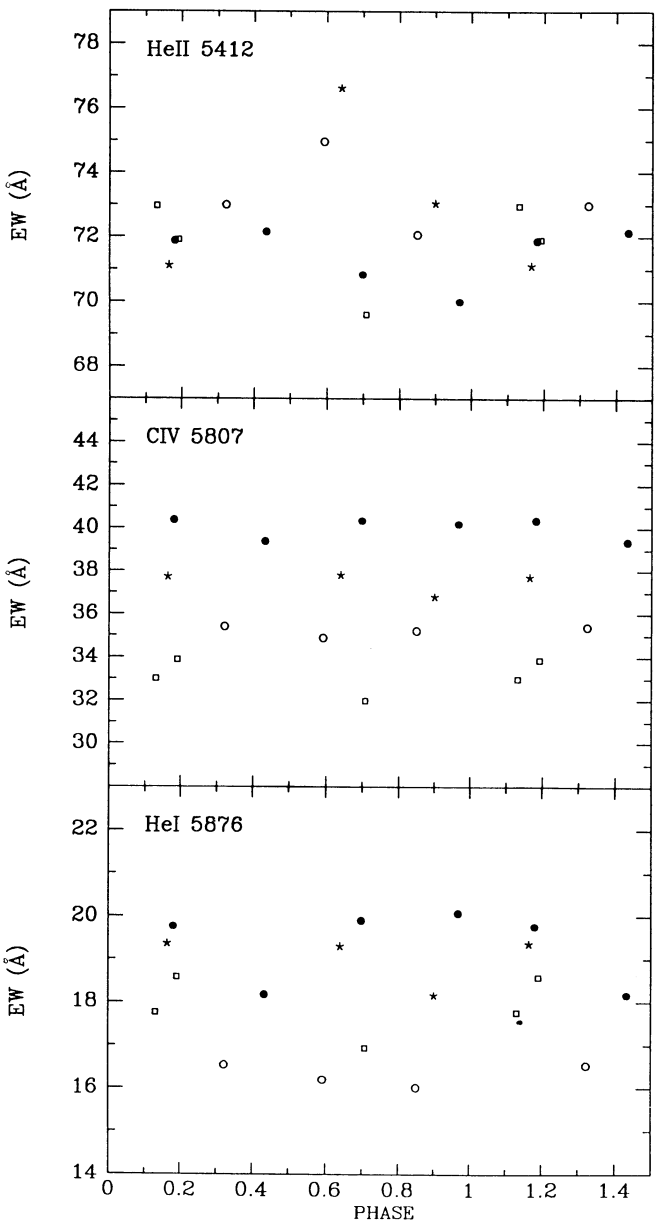

FIG. 16.—Equivalent widths vs. phase for the emission lines He II λ5412, C IV λ5807, and He I λ5876. Phases are as in Fig. 1. Symbols are the same as in Fig. 12.

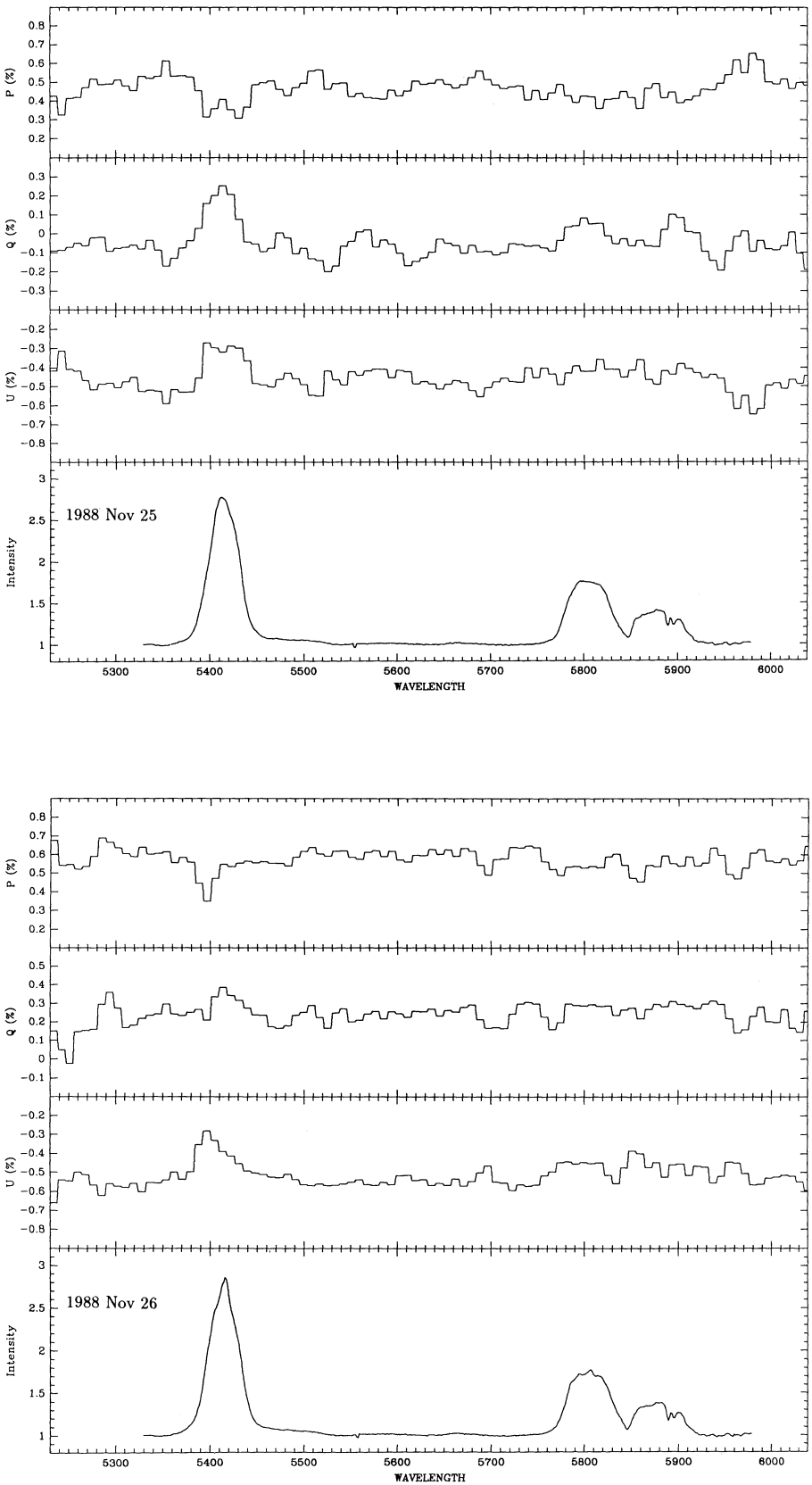

FIG. 17.—Nightly averaged spectropolarimetry from AAT, 1988 November. The Stokes parameters P, Q, and U along with the intensity I are plotted against wavelength (in Å). Polarization data are binned in a 10 Å box. Intensity spectra are truncated in wavelength due to the reduction technique. Note the change of the polarization level in the emission lines.

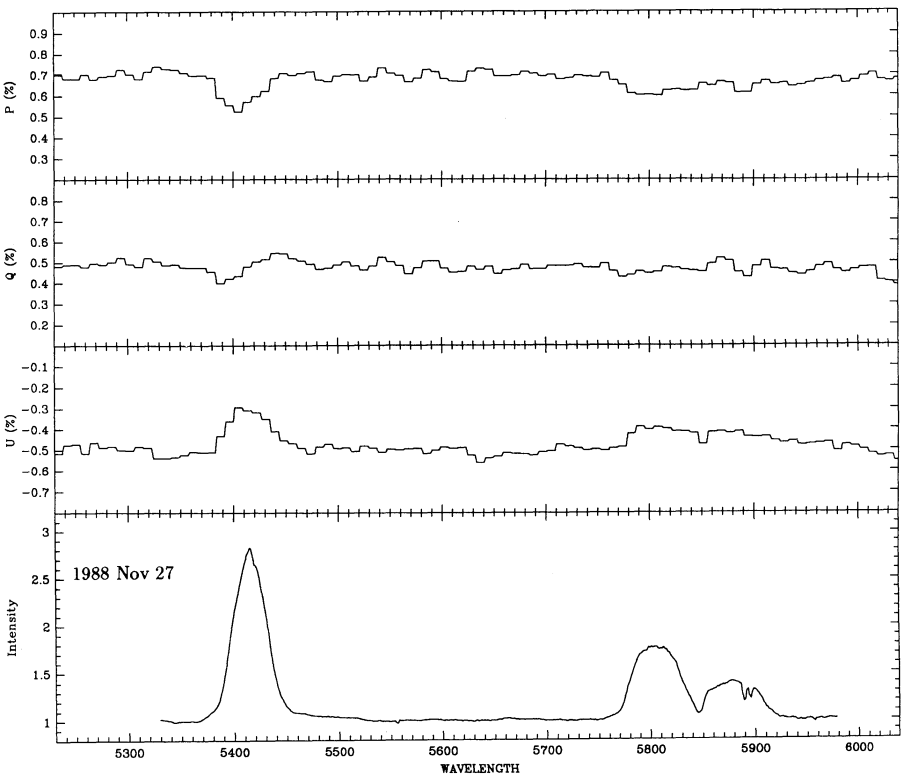

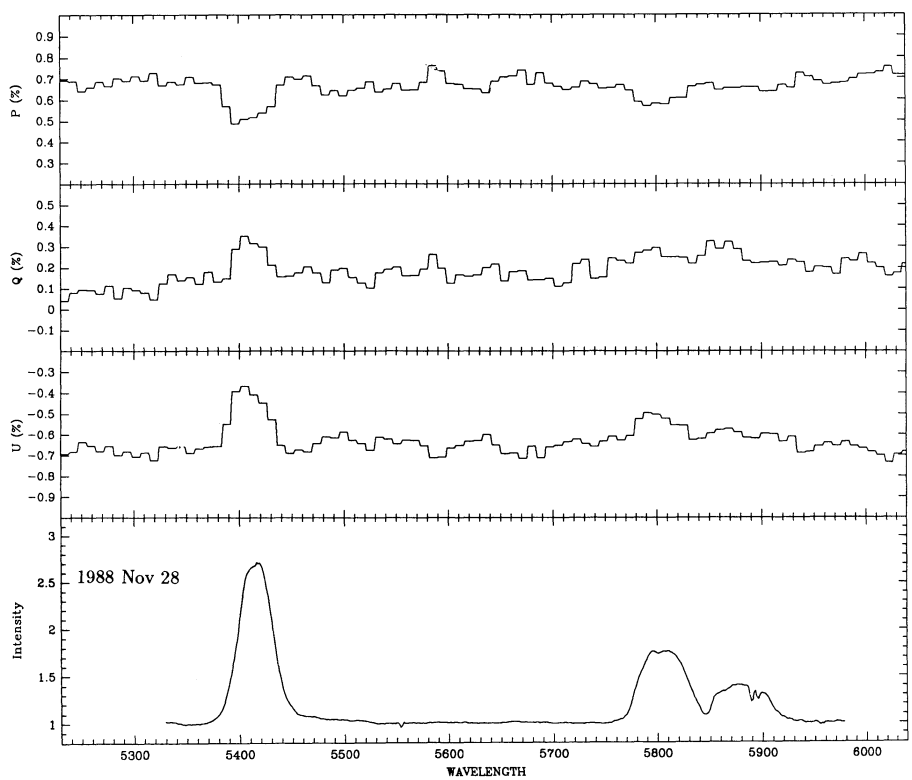

FIG. 17—*Continued*

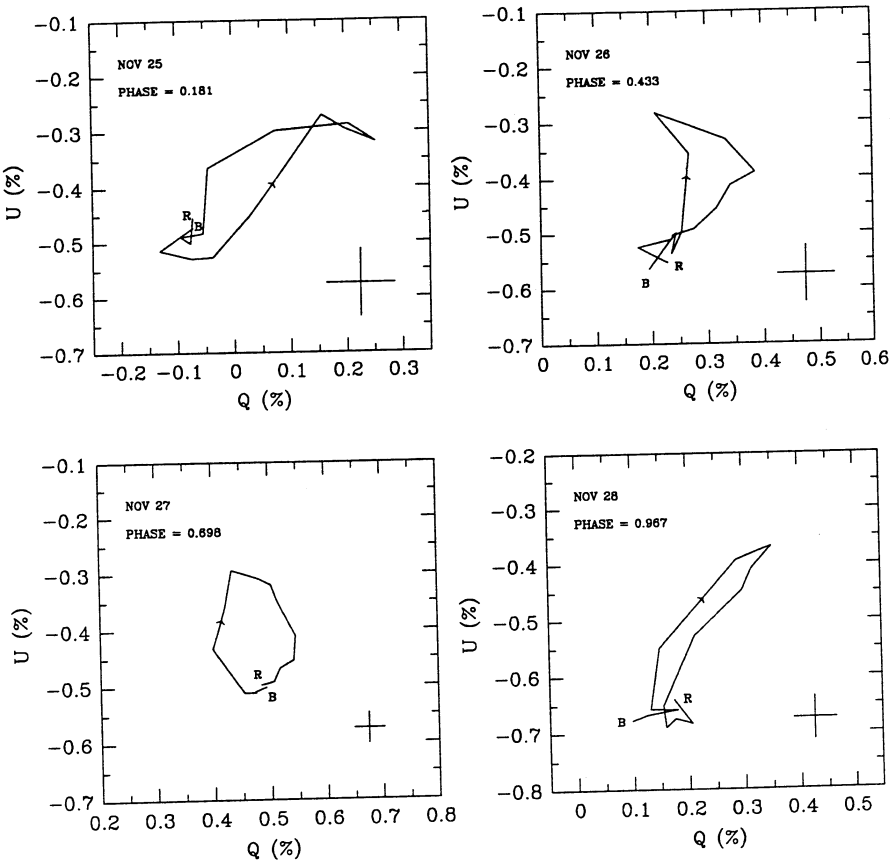

FIG. 18.—Q-U diagram of the polarization across the He II λ5412 emission line for the nightly averaged spectropolarimetry from the AAT, 1988 November. Rotation direction from blue (B) to red (R) is indicated by an arrow. Average 2 σ polarization error in the line is given in the bottom right-hand corner. Phases, according to the LML ephemeris as in Fig. 1, are indicated under the data of observation in the upper left-hand corner. Note the change of the Q-U loop shape and rotation direction with phase.

3.11. *Interstellar Polarization*

Based on the polarization measured in the three emission lines from the AAT spectra (Fig. 17; after removing the continuum flux contribution in the lines), we have estimated, using the empirical interstellar polarization law of Serkowski, Mathewson, & Ford (1975), the interstellar polarization: $P_{max} \approx 0.5\%$, $\theta_{IS} \approx 160°$, and $\lambda_{max} \approx 5600$ Å (the wavelength where the degree of interstellar polarization is maximum). This was done assuming that the lines are totally depolarized compared with the continuum light (see McLean et al. 1979). This may not be strictly the case, however.

These results are consistent with the values obtained by Schulte-Ladbeck et al. (1990). They obtained $P_{max} = 0.55\%$, $\theta_{IS} = 0°$ (i.e., 180°), and $\lambda_{max} = 5500$ Å, based also on spectropolarimetric data. We also plot in Figure 19 the polarization vectors of stars from the catalog of Mathewson et al. (1978) in the region surrounding EZ CMa (i.e., in a circle of radius 10° and within 1 mag of the distance modulus of EZ CMa). This gives an average angle of $\theta_{IS} = 155° \pm 13°$, which is in remarkable agreement with the above results, considering the chaotic nature of the vectors of Figure 19.

3.12. *Correlations among Simultaneous Observations*

The previous sections present independent data for different modes. Here we compare those photometric, polarimetric, and spectroscopic observations which were obtained simultaneously or nearly so.

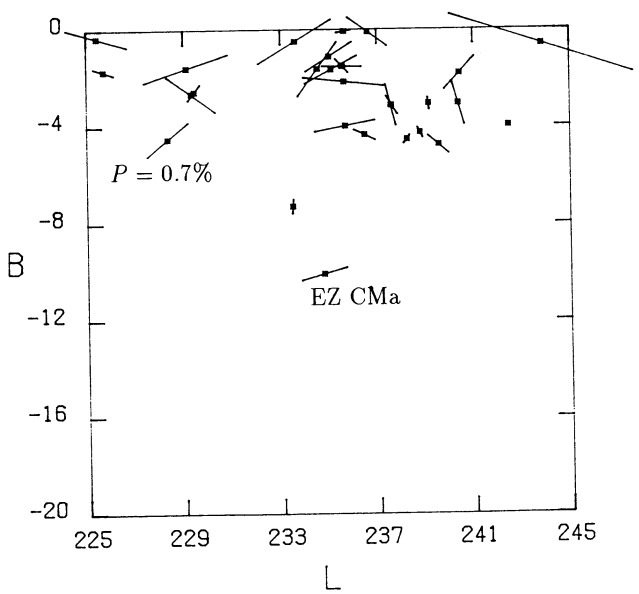

FIG. 19.—Polarization maps for stars in a 20° × 20° region around and within 1 mag in true distance modulus of EZ CMa. The length of the vectors is proportional to the degree of polarization, with the actual value given for a well-isolated star.

Between 1986 and 1990, some photometric and polarimetric data were collected during the same month (see Figs. 1 and 6). First we searched, without success, for a correlation between the shapes of the different curves. Of greater interest is perhaps the change which occurred at phase $\varphi \simeq 0.2$ between the polarimetric curves of 1986 February–April and 1987 February; it coincides well with the sharpening of the light-curve peak of 1987 near the same phase. Unfortunately, no photometric data exist for the period between 1986 and 1987, while the polarimetric curve of 1986 October is quite different. The photometric curve of 1988 October is not very different from the 1987 curve, but the polarimetric curve of 1988 October–November is more difficult to recognize. Finally, in 1990, the polarimetric data show a large amplitude of variation, while the photometric curves become much more complicated, with several local maxima. It seems from this that the correlation between the two modes of variation is certainly not simple. Nevertheless, the time scales for the photometric and polarimetric changes are about the same; during the 3 months of contiguous observations in 1986 and 1990, details in the photometric and polarimetric curves both evolve slowly, in all cases in a continuous fashion. This latter point favors a common mechanism for the two modes of variation.

Unfortunately, the spectroscopic phase coverage is too sparse to allow serious comparison of the profile changes with the polarimetric and photometric curves. (One may wonder whether it is at all meaningful to compare variations in the emission lines with the photometric and polarimetric data, which are mainly due to continuum light, but the truth is that the line profiles do in fact vary!) We compared the average spectra collected on two different nights, but at similar phase ($\varphi = 0.13$ and 0.19), in 1990 February (see Fig. 10) with the UTSO data points obtained simultaneously (Figs. 1 and 6). Even though the two line profiles of He II λ5412 are similar (both have an emission peak on the blue side of the line), they do show some differences. The photometric points also show a change of magnitude: the star is fainter at $\varphi = 0.19$, while the polarimetric data suffer no significant variation. We looked also for a correlation between radial velocity, equivalent width, and $\beta_1^{1/2}$ with the polarimetric and/or photometric curves of 1990 February and 1988 May. Behavior patterns between epochs appear to be quite different. Further intense simultaneous observing runs with good phase coverage are required to continue this important kind of correlation search.

4. DISCUSSION

At the heart of any explanation for the nature of EZ CMa must be the 3.766 day periodicity. Although this object clearly exhibits some degree of random variation on both short and long time scales, this is the only period that is seen consistently in most data sets of high quality that cover several 3.766 day cycles.

4.1. *Nature of the* 3.766 day *Variability*

The only viable explanation for such a long-lasting 3.766 day clock must involve rotation of either a single star whose surface symmetry is broken by a small number of inhomogeneities, or a binary in which the companion is a relatively low-mass (probably compact) object.

Pulsations (radial or nonradial) can be excluded mainly for two reasons: (1) The 3.766 day period is too long (see Moffat & Roberts 1991). (2) The amplitude of variable polarization is much too high compared with the light-curve amplitude to be due to nonradial pulsations (see Moffat 1987). Radial pulsations are not expected to produce any polarization variability.

Although mainly continuum light and polarization data (but also some emission lines, when sufficient high-quality data are available) show the 3.766 day period in a coherent, but often complex, phase diagram at most times, the shape of the phase variations changes, often dramatically, on a time scale of weeks. This lack of long-term coherency might be accounted for by some kind of slow random growth and fading of a small number of disturbances or spots in the visible part of a rotating star. Familiar examples of such objects are T Tauri stars and RS CVn stars. For example, the T Tauri star DN Tau shows light variations which change slowly in amplitude and phase over many rotations (Bouvier, Bertout, & Bouchet 1986). There are also many examples of RS CVn stars with spots migrating and changing on the stellar surface, often in a binary system (e.g., Lodenquai & McTavish 1988; Strassmeier 1990). In many of these stars the modulations (light, radial velocity) are close to *sinusoidal* in shape.

The shape of the light curve of EZ CMa, on the other hand, is often ($\sim$40% of the time) dominated by a rather sharp spike of half-width $\sim$0.2 in phase. At other times, the light curve shows several nearly equal peaks. What kind of spots can prevail in EZ CMa to cause this? Presumably, some kind of constraining, but variable, magnetic loops must be implied (as with the spots on T Tauri or RS CVn stars), since it would otherwise be difficult to explain the fact that one sees in EZ CMa the same period in different levels of the wind, i.e., in lines of different ionization and the continuum. The magnetic field strength must then satisfy the constraint $B^2/8\pi > \frac{1}{2}\rho v_w^2$. With $\rho \simeq m_{\rm He} \times 10^{10}$ g cm^{-3} and $v_w \simeq 10^3$ km s^{-1} in the accelerating part of the wind, this leads to $B > 90$ G.

The same argument would apply to a Be star–like rotating disk: a unique period throughout the disk would require magnetic constraint. The presence of magnetic fields in EZ CMa, however, derives no support from two facts: a lack of intrinsic (variable) circular polarization (Drissen et al. 1989), and no evidence for a nonthermal radio component (Leitherer & Robert 1991). In any case, even a hypothetical rotation period of 3.766 days at the stellar surface ($R_* \simeq 3\,R_\odot$, $M \simeq 10\,M_\odot$, as for the W-R star in the WN6+O6 binary V444 Cyg; Cherepashchuk, Eaton, & Khaliullin 1984) leads to an equatorial rotation velocity $v_e = 2\pi R/P = 40$ km s^{-1}, which is well below the critical rotation velocity $v_{\rm ec} = (GM/R_*)^{1/2} = 800$ km s^{-1}. This makes the creation of a Be star–like disk very unlikely. Nevertheless, Schulte-Ladbeck et al. (1990) have argued in favor of such a configuration in EZ CMa, based on the constant looping in a Q-U plot of linear polarization across the emission lines. However, the new data presented here do reveal a change of direction of the Q-U loop, which complicates the Be interpretation.

On the other hand, some of the light curves of EZ CMa remarkably resemble those of several short-period Be variables that have been studied intensively recently by Balona, Sterken, & Manfroid (1991). At other times, the light curve of EZ CMa shows more than two peaks, less like those Be stars.

Perhaps the strongest argument in favor of a binary system to account for the 3.766 day period is the fact that the (continuum) polarization variability can be fitted by an eccentric orbit model, with a mean eccentricity $e = 0.39 \pm 0.02$ that is close to the eccentricity of the best radial velocity orbital fit: $e = 0.34 \pm 0.08$ (N IV λ3483; Firmani et al. 1980). The form of the polarization curves of EZ CMa are also often quite similar

in both shape and amplitude to polarization curves of the well-known W-R + O binary in the Small Magellanic Cloud, HD 5980, with $e = 0.3$ (Moffat et al. 1992).

The low level of polarization of the emission-line flux from EZ CMa is also what one expects in the case of W-R + O binaries, in which the companion's (mainly continuum) light is scattered by the abundant free electrons in the W-R wind, while the W-R wind emission lines have few asymmetrically located free electrons to scatter off (i.e., the companion's wind is negligible). High-quality spectropolarimetry of known W-R binaries is needed to verify this on a broad scale. The present spectropolarimetric variations of EZ CMa do not contradict a binary model. Furthermore, the loop shape and direction in the *Q-U* plane across the emission lines changes with phase, as expected in a binary, at least qualitatively; however, many more data of high quality are needed to confirm this.

More difficult to explain in the context of a binary is the complex nature of the light curves of EZ CMa. Most W-R + O binaries show a V-shaped depression in their light curves, when the O companion passes behind the W-R star and shines through maximum wind column density (Lamontagne et al. 1992); a few rare cases reveal double minima per orbit due to mutual eclipses. Another possibility to explain especially the sharp peak(s) in the light curve of EZ CMa will be discussed in § 4.2 in the context of a binary system.

Another problem with the binary interpretation is the variable nature of the light and polarization curves (and possibly the line variability) on long time scales. The lack of a clear long period lends little support to binary precession effects, although more data are needed to clarify this. In any case, truly periodic precession could be masked by other sources of variability, such as unpredictable large-scale instabilities in the W-R wind which could distort the accretion disk (e.g., Iping & Petterson 1990).

4.2. *Evidence for a Compact Companion*

Taking the radial velocity orbit of Firmani et al. (1980) for N IV λ3483 W-R emission as the most reliable leads to $K_{WR} \simeq 36 \pm 3$ km s^{-1} and a companion mass of $M_c = 1.3 \pm 0.4\ M_\odot$, assuming $M_{WR} = 10 \pm 5\ M_\odot$ and $i = 71° \pm 3°$. (The present improved inclination $i = 114° \pm 3°$, or $66° \pm 3°$, will increase M_c slightly to $1.4\ M_\odot$.) This corresponds closely to the mean observed mass of NSs in binaries, $1.4\ M_\odot$. It is interesting to note further that the radial velocity orbit of the N V λ4603/λ4620 absorption edges shows higher and variable amplitude, from $K \simeq 130$ to $K \simeq 220$ km s^{-1} (Firmani et al. 1980), with phase shift ~0.3 relative to the emission line N IV λ3483 orbit. Could the N V orbit be more closely associated with the companion NS? Note that one expects a radial velocity amplitude of $36 \times (10/1.4) \simeq 260$ km s^{-1} in antiphase for the companion, neglecting complications due to an eccentric orbit. While some of the N V emission likely arises in the W-R wind, it is conceivable that a certain fraction may come from an ionized cavity around the NS.

If reliable, the existence of an eccentric orbit is unexpected in such a close, massive system, where variable tidal effects should rapidly circularized the orbit (see Tassoul 1990). A plausible way to create an eccentric orbit in a system containing a NS is through a supernova (SN) explosion of the original primary star, leaving a NS remnant. This process is normally expected to produce an OB + NS recoiled runaway binary with high orbital eccentricity (e.g., van den Heuvel 1976). Such a system could evolve in $\sim 10^6$ yr to become W-R + NS, still in an elliptical orbit, as for EZ CMa. Although the isolation and displacement from the Galactic plane of EZ CMa suggest a runaway nature, its radial component of velocity (from its associated ring nebula S308) is not peculiar compared with Galactic rotation at its distance (Pismis & Quintero 1982). Alternatively, the runaway status could be caused by dynamical ejection from a cluster (Leonard & Duncan 1988), in which case EZ CMa would more likely be a single star. Equally intriguing is the fact that EZ CMa may be surrounded by a SNR, if the nearly concentrically distributed high-velocity gas can be shown to be at the same distance as EZ CMa (Nichols-Bohlin & Fesen 1986, 1990).

Can a W-R + NS binary account for the peculiarities of the light curve? If the NS is accreting W-R wind material, it may produce jets à la SS 433. If these jets are also misaligned with the orbital axis, as in SS 433, their interaction with the W-R wind could vary on a long-term scale determined by the precession period. (The ratio of precession to orbital period in SS 433 is ~13; a similar ratio in EZ CMa would yield a precession period of ~50 days.) The collision of the jets with the W-R wind could yield fairly sharp peaks, in view of the $\sim r^{-2}$ falloff in the W-R wind density. Furthermore, if the wind is relatively inhomogeneous as one observes in virtually all W-R stars (Moffat & Robert 1991), accretion may vary with time, producing additional random variability, possibly competing with or even masking the precession-caused modulation. Even if there are no jets, variable accretion or passage of wind material past a magnetic NS could lead to variable light curves.

Another conceivable way to explain the peculiar light curve might be as a result of the passing of photoionization waves (e.g., Blondin et al. 1990) as a NS orbits in the dense W-R wind. Such wakes, if optically thick, could yield at least double light maxima per orbit, when seen broadside.

Could the sharp peak in the light curve be caused by the gravitational lens effect when the W-R star passes directly behind a compact star? Simple calculations based on the work of Refsdal (1964) using the orbit of Firmani et al. (1980) show that one would get a peak of ~1% maximum increase in light for $R_{WR} \simeq 3\ R_\odot$ and $M_c = 1.4\ M_\odot$ for a NS companion. However, the peak would be very much narrower than observed (0.04 versus 0.3 in phase, respectively). A black hole (BH) would improve this, but not by much, unless it were very massive ($M_{BH} \gg 10\ M_\odot$), an unlikely scenario.

On a more empirical level, we note that the shapes of the optical light curves or massive X-ray binaries (MXRBs; OB + c) are often variable over several orbital cycles. In particular, QV Nor (= 4U 1538 − 52; Ilovaisky, Chevalier, & Motch 1979) is such a system, with $P = 3.73$ days and full amplitude ~0.12 mag, in which "the secondary maximum is variable in amplitude by a factor two on a time scale of several binary cycles" (Ilovaisky et al. 1979). A similar phenomenon is seen in LMC X-4 (Chevalier & Ilovaisky 1977), with $P = 1.4$ days and full amplitude ~0.15 mag. Another property often found among MXRBs is that the light-curve scatter is relatively small over 1–2 orbits, but becomes significantly higher when many orbits are combined, as in the case of V884 Sco (= 4U 1700 − 377 = HD 153919; van Paradijs, Hammerschlag-Hensberge, & Zuiderwijk 1978) with $P = 3.4$ days, full amplitude ~0.05 mag. These properties are not unlike those seen in EZ CMa (see combined light curve in Fig. 3 of Drissen et al. 1989).

The main problem with the W-R + c scenario, however, is the lack of significant accretion-type X-ray flux (L_X) as seen in

OB+c binaries. Nevertheless, Pollock (1989) notes that the X-ray variability of EZ CMa on a time scale of months is the highest among all observed W-R stars; L_X also varies on a daily time scale, possibly correlated with orbital phase, as in V444 Cyg (Moffat et al. 1982). If due to colliding winds, as believed in the case of V444 Cyg, this variable X-ray flux would then support a binary hypothesis also in EZ CMa, with the best companion mass corresponding to that of a NS.

Willis et al. (1989) have shown that EZ CMa does not show the Hatchett-McCray ionization effect in the variable behavior of its UV emission lines, as seen in MXRB systems. However, this may not be surprising, since L_X is normal in EZ CMa compared with other W-R stars; possibly the accreting energy is emitted in other modes besides L_X (e.g., Kulkarni & Narayan 1988). This is possible if the accretion disk is optically thick, as in SS 433 (Eggum, Coroniti, & Katz 1988). On the other hand, if the low-mass companion in EZ CMa is a highly magnetized NS, accretion may be very inefficient. Another way to reduce the accretion-type X-ray flux is through a BH instead of a NS (White & Long 1986). However, a BH mass ($\gtrsim 3\ M_\odot$) is not favored by the radial velocity orbit of EZ CMa. Another system of interest is Her X-1, which exhibits high and low states of L_X, depending on orbital phase (Qiao & Cheng 1989). This is likely due to the precession of a tilted accretion disk, which obscures the X-ray source when the disk is in a certain range of orientations. In EZ CMa, such a ring could be in a tilt of permanent occultation.

Another possibly related peculiarity of EZ CMa is the difference between its terminal wind velocity $v_\infty \simeq 1720$ km s^{-1}, based on the bluest part of the saturated ("black") UV resonant P Cygni absorption edges, compared with the P Cygni edge velocity where the blue edge of the absorption meets the continuum, $v_{\rm edge} = 3140$ km s^{-1} (Prinja et al. 1990). This is the largest difference known among all 35 W-R stars given by Prinja et al. (1990); it could be the result of turbulent shocks emanating from a hot, rapidly orbiting NS deep in the W-R wind EZ CMa.

5. CONCLUSION

W-R+c systems are expected to be rare: Moffat (1992) estimated a frequency of $\sim$15%–20% among a complete sample of local W-R stars. This means that only 8–11 of the 51 Galactic W-R stars brighter than $v = 11$ mag (those that have been moderately well studied) are expected to be W-R+c. The unusual properties of EZ CMa suggest that it may be one such case. On the other hand, If EZ CMa is a single star, one is then inclined to wonder why it shows such unique behavior compared to other (single) W-R stars.

In further support of the binary nature of EZ CMa is the following argument: All other W-R stars with known periods *are binaries*; those W-R stars that are not binary, but vary, do so in a stochastic way (see Moffat & Robert 1991). Unless EZ CMa is truly an intrinsic anomaly, most arguments thus favor the binary W-R+c hypothesis. If true, EZ CMa would fill a heretofore missing gap in the evolutionary chain of massive binaries (e.g., Moffat 1982).

The most crucial observations needed at this point in order to tie down the nature of EZ CMa are extensive spectroscopic monitoring. This has been too infrequent and imprecise in the past. Indeed, at the time of writing, just such a world-wide campaign is underway to correlate numerous high S/N spectra with simultaneous photometric and polarimetric variability.

We thank D. Baade for his help with the reduction of the echelle spectra. The authors express their gratitude to the directors of all the observatories visited for the generous allotment of observing time. We also thank the Vatican Observatory for the loan of their polarimeter. Support for the maintenance of the MINIPOL was provided by NSF grant INT82-13103 and grant 0006-85 from the Space Telescope Science Institute. C. R. is grateful for bursaries from the Fonds FCAR of Québec and to the Université de Montréal. A. F. J. M. and L. D. acknowledge financial support from NSERC, Canada.

REFERENCES

Balona, L. A., Egan, J., & Marang, F. 1989, MNRAS, 240, 103
Balona, L. A., Sterken, C., & Manfroid, J. 1991, MNRAS, 252, 93
Blondin, J. M., Kallman, T. R., Fryxel, B. A., & Taam, R. E. 1990, ApJ, 356, 591
Bouvier, J., Bertout, C., & Bouchet, P. 1986, A&A, 158, 149
Brown, J. C., Aspin, C., Simmons, J. F. L., & McLean, I. S. 1982, MNRAS, 198, 787
Brown, J. C., McLean, I. S., & Emslie, A. G. 1978, A&A, 68, 415
Cherepaschuk, A. M. 1981, MNRAS, 194, 765
Cherepaschuk, A. M., Eaton, J. A., & Khaliullin, K. F. 1984, ApJ, 281, 774
Chevalier, C., & Ilovaisky, S. A. 1977, A&A, 59, L9
Chu, Y.-H., Gull, T. R., Treffers, R. R., Kwitter, K. B., & Troland, T. H. 1982, ApJ, 254, 562
Conti, P. S., Leep, E. M., & Perry, D. N. 1983, ApJ, 268, 228
Drissen, L., Robert, C., Lamontagne, R., Moffat, A. F. J., St.-Louis, N., van Weeren, N., & van Genderen, A. M. 1989, ApJ, 343, 426
Ebbets, D. 1979, PASP, 91, 804
Eggum, G. E., Coroniti, F. V., & Katz, J. I., 1988, ApJ, 330, 142
Firmani, C., Koenigsberger, G., Bisiacchi, G. F., Moffat, A. F. J., & Isserstedt, J. 1980, ApJ, 239, 607
Gosset, E., & Vreux, J.-M. 1987, A&A, 178, 153
Hamann, W.-R., Schmutz, W., & Wessolowski, V. 1988, A&A, 194, 190
Hillier, D. J. 1984, ApJ, 280, 744
———. 1985, in IAU Symp. 116, Luminous Stars and Associations in Galaxies, ed. C. W. H. de Loore, A. J. Willis, & P. Laskarides (Dordrecht: Reidel), 261
———. 1987, ApJS, 63, 965
Ilovaisky, S. A., Chevalier, C., & Motch, C. 1979, A&A, 71, L17
Iping, R. C., & Petterson, J. A. 1990, A&A, 239, 221
Kuhi, L. V. 1967, PASP, 79, 57
Kulkarni, S., & Narayan, R. 1988, ApJ, 335, 755
Lamontagne, R., Moffat, A. F. J., Drissen, L., Robert, C., Grandchamp, A., Lapierre, N., & Shara, M. M. 1992, in preparation
Lamontagne, R., Moffat, A. F. J., & Lamarre, A. 1986, AJ, 91, 925 (LML)
Leitherer, C., & Robert, C. 1991, ApJ, 377, 629
Leonard, P. J. T., & Duncan, M. J. 1988, AJ, 96, 222
Lodenquai, J., & McTavish, J. 1988, AJ, 96, 741
Lucy, L. B. 1982, ApJ, 255, 278
Mathewson, D. F., Ford, V. I., Klare, G., Neckel, Th., & Krautter, J. 1978, Bull. Inf. Centre Données Stellaires, 14, 115
McLean, I. S. 1980, ApJ, 236, L149
McLean, I. S., Coyne, G. V., Frecker, J. E., & Serkowski, K. 1979, ApJ, 231, L141
Moffat, A. F. J. 1982, in IAU Symp. 99, Wolf-Rayet Stars: Observations, Physics, Evolution, ed. C. W. H. de Loore & A. J. Willis (Dordrecht: Reidel), 515
———. 1987, in Polarized Radiation of Circumstellar Origin, ed. G. V. Coyne, A. M. Magalhães, A. F. J. Moffat, R. E. Schulte-Ladbeck, S. Tapia, & D. T. Wickramasinghe (Vatican City: Vatican Observatory), 607
———. 1992, A&A, 253, 425
Moffat, A. F. J., Drissen, L., Lamontagne, R., & Robert, C. 1988, ApJ, 344, 1038
Moffat, A. F. J., Firmani, C., McLean, I. S., & Seggewiss, W. 1982, in IAU Symp. 99, Wolf-Rayet Stars: Observations, Physics, Evolution, ed. C. W. H. de Loore & A. J. Willis (Dordrecht: Reidel), 577
Moffat, A. F. J., Niemela, V. S., Seggewiss, W., Magalhães, A. M., & Cerruti, M. A. 1992, in preparation
Moffat, A. F. J., & Robert, C. 1991, in IAU Symp. 143, Wolf-Rayet Stars and Interrelations with Other Massive Stars in Galaxies, ed. K. A. van der Hucht & B. Hidayat (Dordrecht: Kluwer), 109
———. 1992, in ASP Conf. Ser., Vol. 22, Nonisotropic Variable Outflows from Stars, ed. L. Drissen, C. Leitherer, & A. Nota (San Francisco: ASP), 203
Moore, C. E. 1945, A Multiplet Table of Astrophysical Interest (Washington, DC: Department of Commerce, National Bureau of Standards)
Nichols-Bohlin, J., & Fesen, R. A. 1986, AJ, 92, 642

Nichols-Bohlin, J., & Fesen, R. A. 1990, ApJ, 353, 281
Niemela, V. S., & Méndez, R. H. 1982, in IAU Symp. 99, Wolf-Rayet Stars: Observations, Physics, Evolution, ed. C. W. H. de Loore & A. J. Willis (Dordrecht: Reidel), 295
Owocki, S. P., Castor, J. I., & Rybicki, G. B. 1988, ApJ, 335, 914
Pismis, P., & Quintero, A. 1982, in IAU Symp. 99, Wolf-Rayet Stars: Observations, Physics, Evolution, ed. C. W. H. de Loore & A. J. Willis (Dordrecht: Reidel), 305
Pollock, A. M. T. 1989, ApJ, 347, 409
Press, W. H., & Teukolsky, S. A. 1988, Comput. Phys., November/December, 77
Prinja, R. K., Barlow, M. J., & Howarth, I. D. 1990, ApJ, 361, 607
Qiao, G.-J., & Cheng, J.-H. 1989, ApJ, 340, 503
Refsdal, S. 1964, MNRAS, 128, 295
Robert, C. 1992, Ph.D. thesis, Univ. Montréal
St.-Louis, N. 1990, Ph.D. thesis, University College London
St.-Louis, N., Moffat, A. F. J., Drissen, L., Bastien, P., & Robert, C. 1988, ApJ, 330, 286
St.-Louis, N., Willis, A. J., Garmany, C. D., & Conti, P. S. 1991, in IAU Symp. 143, Wolf-Rayet Stars and Interrelations with Other Massive Stars in Galaxies, ed. K. A. van der Hucht & B. Hidayat (Dordrecht: Kluwer), 179
Schmutz, W., Hamann, W.-R., & Wessolowski, U. 1989, A&A, 210, 236
Schulte-Ladbeck, R. E., Nordsieck, K. H., Nook, M. A., Magalhães, A. M., Taylor, M., Bjorkman, K. S., & Anderson, C. M. 1990, ApJ, 365, L19
Serkowski, K. 1970, ApJ, 160, 1083
Serkowski, K., Mathewson, D. S., & Ford, V. L. 1975, ApJ, 196, 261
Shylaja, B. S. 1986, J. Astrophys. Astron., 7, 305
Simmons, J. F. L., & Boyle, C. B. 1984, A&A, 134, 368
Singh, M. 1984, Inf. Bull. Var. Stars, No. 2508
Smith, L. F. 1988, private communication
Smith, L. F., & Kuhi, L. V. 1981, An Atlas of Wolf-Rayet Line Profiles (JILA Rep. No. 117; Boulder: Univ. Colorado)
Smith, L. J., & Willis, A. J. 1982, MNRAS, 201, 451
Stevens, I. R., & Willis, A. J. 1988, MNRAS, 234, 783
Strassmeier, K. G. 1990, ApJ, 348, 682
Tassoul, J.-L. 1990, ApJ, 358, 196
Underhill, A. B., & Yang, K. 1991, ApJ, 368, 588
van den Heuvel, E. P. J. 1976, in IAU Symp. 73, Structure and Evolution of Close Binary Systems, ed. P. Eggleton, S. Milton, & J. Whelan (Dordrecht: Reidel), 35
van der Hucht, K. A., Hudayat, B., Admiranto, A. G., Supelli, K. R., & Doom, C. 1988, A&A, 199, 217
van der Hucht, K. A., van Genderen, A. M., & Bakker, P. R. 1990, A&A, 228, 108
van Genderen, A. M., van der Hucht, K. A., & Steemers, W. J. 1987, A&A, 185, 131
van Paradijs, J. A., Hammerschlag-Hensberge, G., & Zuiderwijk, E. J. 1978, A&AS, 31, 189
Verschueren, W., & Hensberge, H. 1990, A&A, 240, 216
White, R. L., & Long, K. S. 1986, ApJ, 310, 832
Willis, A. J., Howarth, I. D., Smith, L. J., Garmany, C. D., & Conti, P. S. 1989, A&AS, 77, 269
Wilson, O. C. 1948, PASP, 60, 383